2017

Synthesis, characterization and catalytic studies of N-doped ordered mesoporous carbons and functionalized periodic mesoporous organosilicas

Bosky Lalitkumar Parikh
Iowa State University

Synthesis, characterization and catalytic studies of N-doped ordered mesoporous carbons and functionalized periodic mesoporous organosilicas

by

Bosky Parikh

A thesis submitted to the graduate faculty

in partial fulfillment of the requirements for the degree of

MASTER IN SCIENCE

Major: Inorganic Chemistry

Program of Study Committee:
Igor Slowing, Co-Major Professor
Aaron Sadow, Co-Major Professor
Marek Pruski

The student author, whose presentation of the scholarship herein was approved by the program of study committee, is solely responsible for the content of this thesis. The Graduate College will ensure this thesis is globally accessible and will not permit alterations after a degree is conferred.

Iowa State University

Ames, Iowa

2017

DEDICATION

This thesis is dedicated to my parents, Lalitkumar and Nayna Parikh who have been a source of support, motivation, and inspiration throughout my life. A special thanks to my partners in crime; my loving sister, Dhvani Parikh and fiancé, Dhairya Soni for their unconditional love, emotional support, and encouragement that inspired me to work hard and fulfill my dreams.

This work is also dedicated to Melissa Rhodehouse, and Pranjali Naik – friends, sisters, colleagues, and researcher for their understanding and encouragement in the moment of crisis. Both of you have been my best cheerleaders.

TABLE OF CONTENTS

Page

ACKNOWLEDGMENTS iv

ABSTRACT v

CHAPTER 1 GENERAL INTRODUCTION 1
Dissertation organization 1
Introduction 1
References 6

CHAPTER 2 NITROGEN-DOPED ORDERED MESOPOROUS CARBONS: SYNTHESIS, CHARACTERIZATION, AND CATALYSIS 9
Introduction 9
Experimental Section 9
Results & Discussions 15
Conclusions 28
References 29

CHAPTER 3 FUNCTIONALIZED PERIODIC MESOPOROUS ORGANOSILICA: SYNTHESIS, AND CHARACTERIZATION 34
Introduction 34
Experimental Section 36
Results & Discussions 39
Conclusions 45
References 46

CHAPTER 4 SUMMARY AND CONCLUSIONS 49

ACKNOWLEDGMENTS

I would like to express my sincere gratitude to my advisor Prof. Igor Slowing for the continuous support of my graduate study, and providing me with an excellent environment for doing research. I thank him for his continuous patience, motivation, immense knowledge, and all the opportunities that were given to conduct my research. I am extremely lucky to have a supervisor who responded to my questions and queries promptly.

Besides my advisor, I would like to thank rest of my committee members Dr. Aaron Sadow and Dr. Marek Pruski for insightful comments and valuable guidance. A special thanks to Dr. Aaron Sadow, who gave me access to his research facilities. I would also like to thank our former post doc and a friend – Dr. Naftali Opembe for training me when I was a new-comer and for pearls of wisdom and expertise that greatly assisted me during research. A very special thanks to my friends Younghun Park, Dilini Singappuli, and Umesh Chaudhary, who were always willing to help and give best suggestions. A special thanks to my friend Raghu Maligal-Ganesh for his time and thoughtful insights during my prelims.

I would also like to thank Dr. Wenyu Huang for letting me use their ICP-MS in the moment of crisis. A special thanks to Mr. Matt Besser for letting me use XRD. I would like to thank Dapeng Jing for performing XPS analysis, Steve Veysey for performing CHN elemental analysis, Sebastián Manzano for performing TEM analysis, Deyny Mendivelso for performing Raman analysis.

Finally, I would like to thank US Department of Energy, Ames Laboratory for funding the projects.

ABSTRACT

Ordered porous materials are crucial and ubiquitous in fundamental research and many practical applications such as catalysis, adsorption, separation, and sensing due to their unique properties such as high surface areas, large pore volumes, and narrow and tunable pore size distributions. The primary focus of this work was the synthesis of two different types of mesoporous materials: nitrogen-doped ordered mesoporous carbon (N-OMC) and functionalized periodic mesoporous organosilica (PMO), their characterization and their potential applications.

My research on N-OMC is focused on its synthesis, characterization, and its use as an active catalyst for hydrogenation of nitrobenzene. In this study, N-OMC were synthesized via polycondensation of 3-aminophenol and formaldehyde templated by self-assembled Pluronic F127 micelles in basic medium. The material was carbonized at various temperatures to control nitrogen content (%N) and degree of graphitization. The goal of this study is to evaluate the effects of nitrogen-doping of OMC on the catalytic activity of supported Pd towards the selective hydrogenation of nitroarenes. Our study suggests that Pd-N-OMC showed better catalytic activity for hydrogenation of nitrobenzene than Pd-OMC. The better catalytic activity of Pd-N-OMC can be attributed to formation of small Pd nanoparticles and uniform distribution.

The research on PMO is focused on the synthesis of ethylene and phenylene bridged PMO functionalized with various organic groups. The materials were synthesized via co-condensation between organo-mono-silanes and organo-bis-silanes. The parent- and functionalized-EPMO, and BPMO materials exhibited high surface area, pore volume, and pore sizes. We believe these functional materials have ideal properties for advanced applications such as interfacial catalysis and selective adsorption.

CHAPTER 1
GENERAL INTRODUCTION

Dissertation Organization

The thesis is organized in four chapters. Chapter 1 is a general introduction and provides insight about routes to synthesize ordered mesoporous carbons (OMCs) and periodic mesoporous organosilicas (PMOs). After a brief overview, Chapter 2 focuses on the synthesis, characterization, and catalytic application of nitrogen doped ordered mesoporous carbons (N-OMCs). Chapter 3 discusses the synthesis and characterization of periodic mesoporous organosilicas (PMOs) functionalized with various organic groups. To finish, Chapter 4 summarizes the thesis.

Introduction

Ordered porous materials are crucial and ubiquitous in fundamental research and many practical applications such as catalysis, adsorption, separation, and sensing due to their unique properties such as high surface areas, large pore volumes, and narrow and tunable pore size distributions.[1,2,3,4] According to their pore diameter, materials can be categorized into microporous (<2 nm), mesoporous (2-50 nm), and macroporous (>50 nm).[5] Microporous materials such as zeolites, activated carbons, carbon molecular sieves, and microporous silica are mostly used in applications such as adsorption, separation, and catalysis.[6,7,8] Despite their high surface area and their wide-spread applications, there are some key drawbacks such as slow mass transport, collapse of porous structures at high temperatures, low conductivity due to defects, low diffusion capacity, and failure to accommodate bulky compounds.[9,10] On the other hand, macroporous materials such as carbon nanotubes and macroporous silica materials tends to have lower surface areas.[11,12] Due to these disadvantages of micro and macroporous materials,

development of mesoporous materials is desirable. This chapter focuses on the synthetic procedures of two classes of mesoporous materials and the influence of their properties on catalysis.

N-doped ordered mesoporous carbons (N-OMC):

In addition to the properties of porous materials, OMC have high stability to hydrolytic conditions, low density, electrical conductivity, and have been used as supports for catalysts, adsorbents for non-polar species, capacitors, and electrodes.[13,14,15]

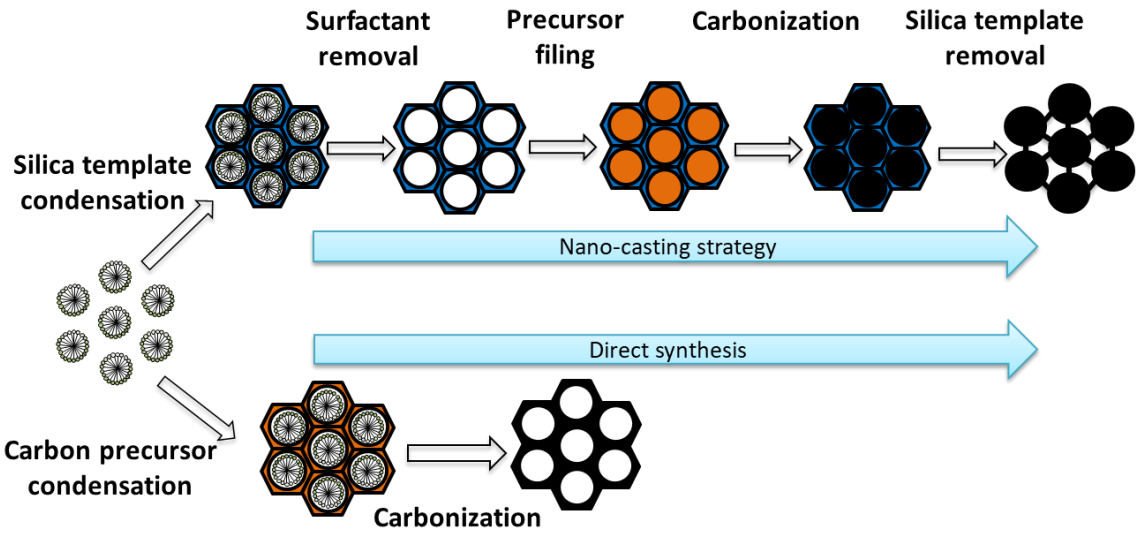

Figure 1: Routes to synthesize OMC materials: nanocasting (top route) and direct synthesis (bottom route)

Hard- (nanocasting) and soft-templating (direct synthesis) are the two traditional routes to synthesize OMCs (Fig.1).[16] In nanocasting route, a pre-synthesized mesoporous silica templates such as SBA-15, FDU, KIT, or MCM-48 is used as a structure directing agent (SDA) to achieve various pore organizations such as 2D-hexagonal, and 3D-cubic.[17,18,19,20] The carbon-precursors are then impregnated inside the pores of silica template followed by carbonization under inert atmosphere. The silica template is then etched yielding the OMC product. The drawbacks of nanocasting are that it requires a sacrificial template, hazardous conditions for removal of silica

template, is time-consuming, and unsuitable for large-scale production. The alternative soft-templating route to synthesize OMC relies on non-covalent interactions between a co-block polymer SDA and a carbon-precursor to form ordered mesophases that undergo thermal polymerization to give continuous frameworks. The pyrolysis of the SDA-polymer under inert atmosphere decomposes and removes the template and carbonizes the polymer to finally produce OMC.[21,22,23] The wide range applications of OMC doesn't only depend on the high porosity of the materials but also relies on the heteroatom doped within the carbon framework.

The electronic and chemical properties of porous carbons can be tuned by doping various elements such as nitrogen, boron, and phosphorus.[24,25] Among these, nitrogen is the most widely doped element in the porous carbon framework. Post-synthetic treatment and hard-templating are the two most common methods to dope nitrogen into porous carbons.[26] However, the post-synthetic route gives non-uniform distributions of nitrogen functionalities while the hard-templating route is hazardous and time-consuming. Thus, there is a need to prepare N-doped OMCs using a direct-synthesis route. In chapter 2, we will discuss a new route to directly synthesize N-OMCs and the effect of nitrogen functionalities on catalysis.

Periodic mesoporous organosilicas (PMOs):

Researchers from Mobil corporation in 1992 synthesized mesoporous silica (M41S) by using cationic surfactant (alkyltrimethyl ammonium halides) as a structure directing agent (SDA) for different silica precursors.[27,28] The resulting material had periodic pore arrangement, amorphous pore walls, and pore size ranging between 1.5-10 nm.[27] Later, Stucky and co-workers synthesized mesoporous silica thin films with large pore size around 9.0 nm using block copolymer of ethylene oxide (EO) and propyleneoxide (PO) as SDA.[29] After these breakthroughs in template directed synthesis of mesoporous silica, considerable efforts have been devoted

towards the synthesis of mesoporous silica with different morphologies such as 2D-Hexagonal, cubic, and lamellar.[27,30] All these materials possess physicochemical properties such as high surface areas, pore volumes and tunable pore sizes. Due to these properties, the materials have been extensively used in several applications such as catalysis, adsorption, host inclusion chemistry, and separation science.[31] Functionalization of these materials using organic groups or impregnation of metal can further increase their potential in certain applications. The functionalization of organic groups can be performed via grafting or condensation reaction.[31] Though, functionalized mesoporous silica suffers from some drawbacks such as heterogeneous distribution of functionalities, and decrease in surface area and pore volume upon high loadings of organic groups.[31] Therefore, synthesis of another class of mesoporous material is required.

Periodic mesoporous organosilica (PMOs) belongs to a class of mesoporous silica that possesses organic-inorganic composites (Fig. 2a).[32,33] PMOs have an organic bridging group covalently bonded to two or more silicon atoms.[33] As shown in Fig. 2, PMOs can be synthesized using different pathways: via condensation of (1) single organo-bis-silane precursors (2) two or more organosilane precursors, or (3) an organo-bis-silane precursor and organosilane.[33] In all of these pathways, organo-bis-silane and organic functional group undergo hydrolysis and polycondensation while interacting with SDA to form mesoporous composites. The composites are subsequently treated to remove the SDA via solvent extraction to give the final PMO.[34] By choosing appropriate organic bridging groups, the physical and chemical properties of PMOs can be tuned. Chapter 3 discusses the synthesis and characteristics of PMOs prepared via co-condensation of organo-bis-silane precursors and organosilane.[35]

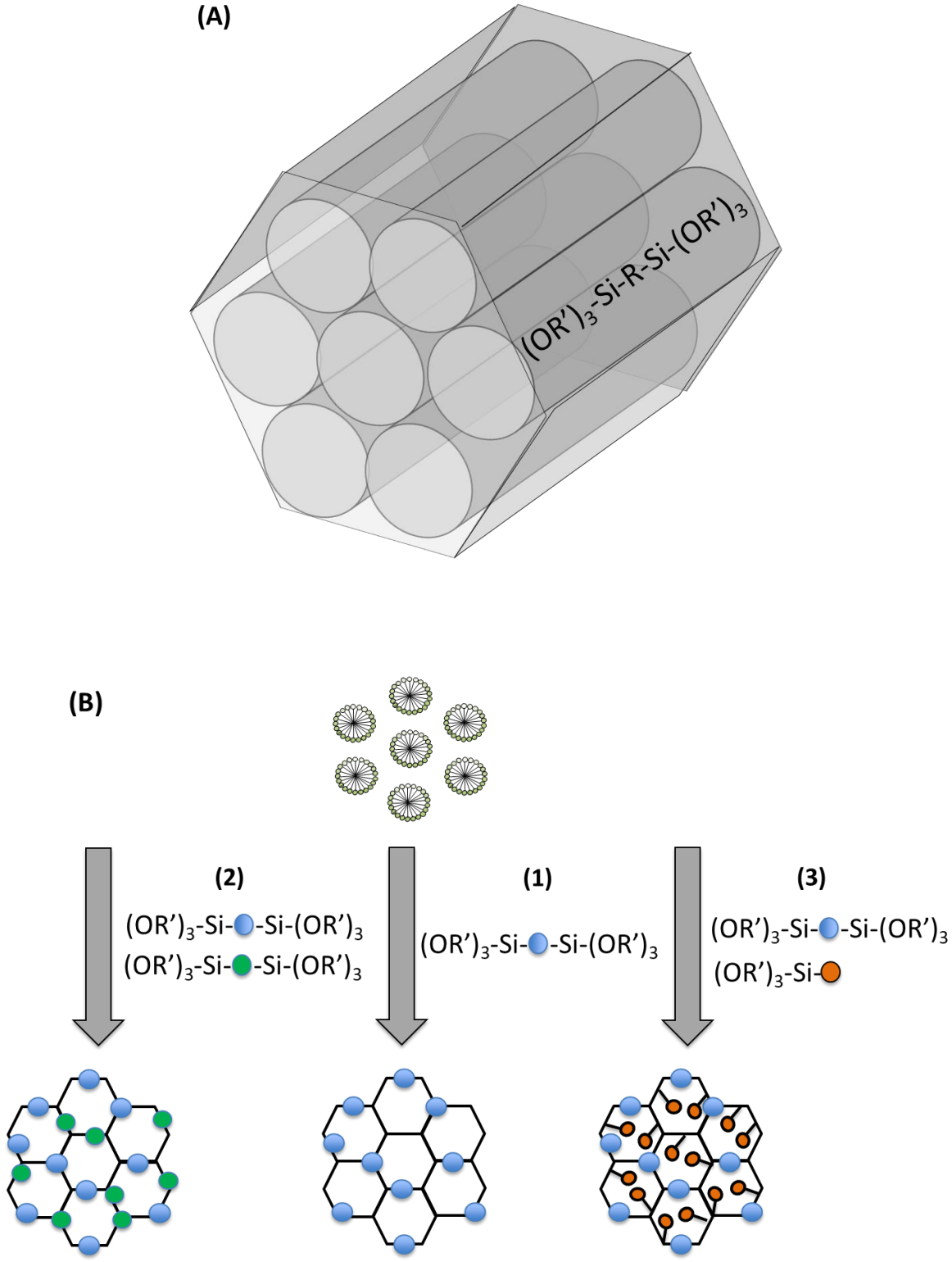

Figure 2: (A): Generic structure of PMOs.[36] R = bridging group, R'= methyl or ethyl group, (**B):** various pathways to synthesize PMOs[37]

References

[1] Ying, J.; Mehnert, C.; Wong, M. Synthesis and Application of Supramolecular-Templated Mesoporous Materials, *Angew. Chem. Int. Ed.*, **1999**, *38*, 56-77.

[2] Davis, M. Ordered Porous Materials for Emerging Applications, *Nature*, **2002**, *417*, 813-821.

[3] Zhang, J.; Liu, X.; Blume, R.; Zhang, A.; Schlögl, R.; Su, D. Surface-Modified Carbon Nanotubes Catalyze Oxidative Dehydrogenation of n-Butane, *Science*, **2002**, *322*, *5898*, 73-77.

[4] Eftekhari, A.; Fan, Z. Ordered Mesoporous Carbon and its Applications for Electrochemical Energy Storage and Conversion, *Mater. Chem. Front.*, **2017**, *1*, 1001-1027.

[5] Kresge, C.; Leonowicz, M.; Roth, W.; Vartuli, J.; Beck, J. Ordered Mesoporous Molecular Sieves Synthesized by a Liquid-Crystal Template Mechanism, *Nature*, **1992**, *359*, 710-712.

[6] Minachev, K.; Isakov, Y. Catalytic Properties of Zeolites – A General Review, *Am. Chem. Soc.*, **1973**, 451-460.

[7] Bhatnagar, A.; Hogland, W.; Marques, M.; Sillnpää, M. An Overview of The Modification Methods of Activated Carbon for its Water Treatment Applications, *Chem. Eng. J.*, **2013**, *219*, 499-511.

[8] Rishidi, A.; Kazemi, D.; Izadi, N.; Pourkhalil, M.; Jorsaraei, A.; Ganji, E.; Lotfi, R. Preparation of Nanoporous Activated Carbon and its Application as Nano Adsorbent for CO_2 Storage, *Korean. J. Chem. Eng.*, **2016**, *33*, *2*, 616-622.

[9] Perot, G.; Guisnet, M. Advantages and Disadvantages of Zeolites as Catalysis in Organic Chemistry, *J. Mol. Cat.*, **1990**, *61*, 173-196.

[10] Liang, C.; Li, Z.; Dai, S. Mesoporous Carbon Materials: Synthesis and Modification, *Angew. Chem. Int. Ed.* **2008**, *47*, 3696–3717.

[11] Galarneau, A.; Calin, N.; Iapichella, J.; Barrande, M.; Denoyel, R.; Coasne, B.; Fajula, F. Optimization of the Properties of Macroporous Chromatography Silica Supports Through Surface Roughness Control, *Chem. Mater.*, **2009**, *21*, 1884-1892.

[12] Prasek, J.; Drbohlavova, J.; Chomoucka, J.; Hubalek, J.; Jasek, O.; Adam, V.; Kizek, R. Methods for Carbon Nanotubes Synthesis – Review, *J. Mat. Chem.*, **2011**, *21*, 15872-15884.

[13] Xia, Y.; Yang, Z.; Mokaya, R. Templated Nanoscale Porous Carbons, *Nanoscale*, **2010**, *2*, 639-659.

[14] Lee, J.; Yoon, S.; Hyeon, T.; Oh, S.; Kim, K. Synthesis of a New Mesoporous Carbon and its Application to Electrochemical Double-Layer Capacitors, *Chem. Comm.*, **1999**, 2177-2178.

[15] Sakintuna, B.; Yürüm, Y. Templated Porous Carbons: A Review Article, *Ind. Eng. Chem. Res.*, **2005**, *44*, *9*, 2893–2902.

[16] Ma, T.; Liu, L.; Yuan, Z. Direct Synthesis of Ordered Mesoporous Carbons, *RSC. Adv.*, **2013**, *42*, 3977-4003.

[17] Zhao, D.; Feng, J.; Huo, Q.; Melosh, N.; Fredrickson, G.; Chmelka, B.; Stucky, G. Triblock Copolymer Syntheses of Mesoporous Silica with Periodic 50 to 300 Angstrom Pores, *Science*, **1998**, *279*, 548-552.

[18] Kim, T.; Kleitz, F.; Paul, B.; Ryoo, R. MCM-48-Like Large Mesoporous Silicas with Tailored Pore Structure: Facile Synthesis Domain in a Ternary Triblock Copolymer-Butanol-Water System, *J. Am. Chem. Soc.*, **2005,** *127*, *20*, 7601–7610.

[19] Kruk, M.; Dufour, B.; Celer, E.; Kowalewski, T.; Jaroniec, M.; Matyjaszewski, K. Synthesis of Mesoporous Carbons using Ordered and Disordered Mesoporous Silica Templates and Polyacrylonitrile as Carbon Precursor, *J. Phys. Chem. B*, **2005**, *109*, *19*, 9216-9225.

[20] Dia, W.; Zheng, M.; Zhai, Y.; Liao, S.; Ji, G.; Cao, J. Templated Synthesis of Three-Dimensional Cubic Ordered Mesoporous Carbon with Tunable Pore Sizes, *Nano. Res. Lett.*, **2010**, *5*,103–107.

[21] Meng, Y.; Gu, D.; Zhang, F.; Shi, Y.; Yang, H.; Li, Z.; Yu, C.; Tu, B.; Zhao, D. Ordered Mesoporous Polymers and Homologous Carbon Frameworks: Amphiphilic Surfactant Templating and Direct Transformation, *Angew. Chem. Int. Ed.*, **2005**, *44*, 7053 –7059.

[22] Tanaka, S.; Nishiyama, N.; Egashira, Y.; Ueyama, K. Synthesis of Ordered Mesoporous Carbons with Channel Structure from an Organic-Organic Nanocomposite, *Chem. Commun.*, **2005**, 2125–2127.

[23] Liang, C.; Hong, K.; Guiochon, G.; Mays, J.; Dai, S. Synthesis of a Large-Scale Highly Ordered Porous Carbon Film by Self-Assembly of Block Copolymers, *Angew. Chem. Int. Ed.*, **2004**, *43*, 5785 –5789.

[24] Terrones, H.; Lv, R.; Terrones, M.; Dresselhause, M. The Role of Defects and Doping in 2D Graphene Sheets and 1D Nanoribbons, *Rep. Prog. Phys.*, **2012,** *75*, 062501.

[25] Medjanik, K.; Chercka, D.; Nagel, P.; Merz, M.; Schuppler, S.; Baumgarten, M.; Muellen, K.; Nepijko, S. A.; Elmers, H.; Schoenhense, G.; Jeschke, H.; Valenti, R. Orbital-Resolved Partial Charge Transfer from the Methoxy Groups of Substituted Pyrenes in Complexes with Tetracyanoquinodimethane-A NEZAFS Study, *J. Am. Chem. Soc.*, **2012**, 134, 4694-4699.

[26] Shen, W.; Fan, W. Nitrogen-containing Porous Carbons: Synthesis and Application, *J. Mat. Chem. A*, **2013**, *1*, 199-1013.

[27] Kresge, C.; Lenowicz, M.; Roth, W.; Vartuli, J.; Beck, J. Ordered Mesoporous Molecular Sieves Synthesized by a Liquid-Crystal Template Mechanism, *Nature*, **1992**, *359*, 710-712.

[28] Beck, J.; Vartuli, J.; Roth, W.; Leonowicz, M.; Kresge, C.; Schmitt, K.; Chu, C.; Olson, D.; Sheppard, E., A New Family of Mesoporous Molecular Sieves Prepared with Liquid Crystal Templates, *J. Am. Chem. Soc.*, **1992**, *114*, 10834-10843.

[29] Zhao, D.; Yang, P.; Melosh, N.; Feng, J.; Chmelka, B.; Stucky, G. Continuous Mesoporous Silica Films with Highly Ordered Large Pore Structures, *Adv. Mat.*, **1998**, *10*, 1380-1385.

[30] Øye, G.; Sjöblom, J.; Stöcker, M. Synthesis, Characterization and Potential Applications of New Materials in the Mesoporous Range, *Adv. Colloid Interface Sci.*, **2001**, *89*, 439-466.

[31] Huo, Q.; Margolese, D.; Stucky, G. Surfactant Control of Phases in the Synthesis of Mesoporous Silica-Based Materials, *Chem. Mater.*, **1996**, *8*, 1147-1160.

[32] Liang, Z.; Mohanty, P; Fei, Y.; Landskron, K. Synthesis of Corsite Nanocrystals from Ethane Bridged Periodic Mesoporous Organosilica at Low Temperature and Extreme Pressure, *Chem. comm.*, **2010**, *46*, 8815-8817.

[33] Hatton, B.; Landskron, K.; Whitnall, W.; Perovic, D.; Ozin, G. Past, Present and Future of Periodic Mesoporous Organosilica – The PMOs, *Acc. Chem. Res.* **2005,** *38,* 305-312.

[34] Hoffmann, F.; Cornelius, M.; Morell, J.; Fröba, M. Silica-Based Mesoporous Organic–Inorganic Hybrid Materials, *Angew. Chem. Int. Ed.*, **2006**, *45*, 3216-3251.

[36] Wang, W.; Lofgreen. J.; Ozin, G. Why PMO? Towards functionality and Utility of Periodic Mesoporous Organosilicas, *Small.* **2010**, *6, 23*, 2634-2642.

[37] Park, S.; Moorthy, M.; Ha, C. Periodic Mesoporous Organosilicas for Advanced Applications, *NPG Asia Mat.*, **2014**, *6*, 1-20.

CHAPTER 2

NITROGEN-DOPED ORDERED MESOPOROUS CARBONS: SYNTHESIS, CHARACTERIZATION, AND CATALYSIS

In this study, nitrogen-doped ordered mesoporous carbons (N-OMC) were synthesized via polycondensation of 3-aminophenol and formaldehyde templated by self-assembled Pluronic F127 micelles in basic medium. Hexamethylenetetramine (HMT) was used as a source of formaldehyde during the condensation reaction. The material was carbonized at various temperatures to control nitrogen content (%N) and degree of graphitization. N-OMC was studied as a support for catalytic palladium nanoparticles, prepared via incipient wetness impregnation. The goal of this study is to evaluate the effects of nitrogen-doping of OMC on the catalytic activity of supported Pd towards the selective hydrogenation of nitroarenes. Pd-N-OMC showed better catalytic activity for hydrogenation of nitrobenzene than Pd-OMC. The better catalytic activity of Pd-N-OMC can be attributed to formation of small Pd nanoparticles and uniform distribution.

Introduction

The catalytic hydrogenation of nitrobenzene is an important process for the large scale production of anilines used in industries such as pharmaceutical, automobile, and construction.[1,2] Aniline and its derivatives can be used in various applications such as dyes, in the production of polyurethane, rubber processing chemicals, polymer surfactants, and pesticides.[3,4,5,6] Many homogeneous and heterogeneous nitrobenzene hydrogenation catalysts have been synthesized using metals such as ruthenium, platinum, palladium, rhodium, iridium, and their oxides.[2,7,8] In general, palladium catalysts supported on carbon materials show good selectivity and catalytic

activity for hydrogenation of nitrobenzene. Typical supports include activated carbon fibers, carbon black, activated carbon cloths, carbon nanofibers and carbon nanotubes.[9,10,11,12,13,14]

Porous carbons have unique properties such as high surface area, thermal stability, chemical inertness, wettability, and electric conductivity.[15,16,17] The electronic and physical properties of carbon materials can be tuned via doping of nitrogen atom. Because of such changes these materials have gained lot of attention in the field of catalysis, gas adsorption, and as supercapacitors.[16,17,18] Zhao and co-workers observed that incorporation of nitrogen atoms within carbon materials increases its capacitance and electronic conductivity.[19,20] Boehm and co-workers observed an increase in catalytic activity for oxidation and hydrogen halide elimination reaction upon nitrogen doping.[21] Zhao and Shin's groups independently synthesized nitrogen-doped porous carbon materials and observed higher catalytic activity for oxygen reduction reaction.[22,23] Jagdeesh and co-workers observed higher dispersion of iron metal nanoparticles with nitrogen doping on carbon framework.[24] From these reports, it is evident that the catalytic activity of catalysts supported on carbons can be affected by nitrogen doping, likely through interactions with the support that control the metal particle size and dispersion, and the electronic properties of the catalyst.

Among two traditional routes to synthesize carbon materials, in post-synthetic treatment, incorporation of nitrogen functionalities within carbon framework can be conducted using heat treatment in the presence of nitrogen containing reagents.[18] Ammonia, pyridine, nitric acid, urea, hydrogen cyanide, and amines are the common nitrogen containing reagents used for this purpose.[25,26,27,28,29,30] However, post-synthetic treatment causes non-homogeneous distribution of nitrogen entities in the carbon framework.[31] Thus, hard-templating is considered a more favorable route to synthesize N-OMCs. The most common precursors used in this technique are

melamine-formaldehyde, urea, acrylonitrile, and pyrrole.[32,33,34,35] Although a lot of research has been conducted on synthesis of nitrogen doped porous carbon, the procedure is time-consuming, requires hazardous conditions and is expensive. Therefore, researchers have started synthesizing N-OMC using soft-templating methods.

Wan and co-workers synthesized N-OMC via evaporation induced self-assembly (EISA) using melamine, formaldehyde and phenol as the carbon-nitrogen precursors and Pluronic F127 as structure directing agent.[36] Yang and co-workers also synthesized nitrogen-doped mesoporous carbon using urea-phenol-formaldehyde resin via EISA method.[37] Recently, Yu and co-workers synthesized N-OMC using resorcinol and melamine as the carbon and the carbon-nitrogen precursors respectively. They used hexamethylenetetramine (HMT) as formaldehyde source to control the polymerization kinetics.[38] The same group also synthesized N-OMC using urea as the carbon-nitrogen source.[39] Wang's group reported the first synthesis of N-OMC with 2D-hexagonal mesopore structure using 3-aminophenol and resorcinol as the carbon-nitrogen and the carbon precursors, respectively.[40] Additionally, Shen's group recently reported the synthesis of N-OMC with cubic mesopore structure using 3-aminophenol as the carbon-nitrogen precursor in presence of HMT.[41]

Inspired by these studies, we have synthesized ordered mesoporous carbon (OMC) and N-OMC and used them as supports for catalytic Pd nanoparticles. The effect of nitrogen doping on the activity of the supported catalysts was studied using nitrobenzene hydrogenation as a test reaction.

Experimental Section

Reagents: Pluronic F127, hexamethylenetetramine, resorcinol, 3-aminophenol, mesitylene (TMB), palladium(II) nitrate dihydrate $Pd(NO_3)_2{\cdot}2H_2O$, and 4-nitrophenol were purchased from

Sigma Aldrich. Ammonium hydroxide, nitrobenzene and aniline were purchased from Fisher. All the reagents were used as received without further purification.

Synthesis of OMC: The synthesis was adapted from the previously reported method.[42] Pluronic F127 (2.00 g), HMT (0.70 g, 5.00 mmol), resorcinol (1.10 g, 10.0 mmol), and mesitylene (0.40 g, 3.33 mmol) were dissolved in deionized water (52 mL) and ammonium hydroxide (14.8 M, 2.0 mL). The contents were stirred to dissolve at room temperature for 1 h. The resultant solution changed its color to dark green. The mixture was transferred into pre-heated oil bath (80 ^{o}C, 200 rpm) and was stirred for 24 h. The mixture was cooled down using an ice bath and a solid product (brown color) was obtained via centrifugation (8000 rpm, 40 min). The material was air-dried at room temperature. The as-synthesized material was further carbonized at various temperatures (300, 400, 500, and 600 ^{o}C) at a heating rate of 1 ^{o}C min^{-1} under nitrogen flow for 6 h. The final products were labeled as OMC-T (T=carbonization temperature).

Synthesis of N-OMC: In a typical synthesis of N-OMCs, Pluronic F127 (2.00 g), HMT (0.70 g, 5.00 mmol), 3-aminophenol (1.08 g, 10.0 mmol), and mesitylene (0.40 g, 3.33 mmol) were dissolved in deionized water (52 mL) and ammonium hydroxide (14.8 M, 1.0 mL). The contents were stirred to dissolve at room temperature for 1 h. The resultant solution changed its color to yellowish-green. The mixture was transferred into a pre-heated oil bath (80 ^{o}C, 200 rpm) and was stirred for 24 h. The mixture was cooled down using an ice bath and the solid product (brown color) was obtained via centrifugation (10000 rpm, 40 min). The material was then air dried at room temperature. The as-synthesized material was further carbonized at various temperatures (300, 400, 500, and 600 ^{o}C) at a heating rate of 1 ^{o}C min^{-1} under nitrogen flow for 6 h. The final products were labeled as N-OMC-T (T=carbonization temperature).

Synthesis of catalysts (Pd-OMC-T, Pd-N-OMC-T): All the catalysts were prepared by incipient wetness impregnation of palladium(II) nitrate dihydrate salt. $Pd(NO_3)_2{\cdot}2H_2O$ (75.1 mg, 0.281 mmol) was dissolved in acetone (2.0 mL) for each carbon support (925 mg). The carbon support was placed in a mortar and the palladium salt solution was added in portions corresponding to the pore volume of the material. The solution was mixed with the support using a pestle, thoroughly ground, and was oven dried between each portion. The impregnated palladium salt was then reduced using $NaBH_4$/EtOH (10.6 mM) solution. For each gram of support, 5.0 mL of $NaBH_4$/EtOH solution was stirred at room temperature for 1 h. The material was then washed using ethanol to obtain Pd supported OMC or N-OMC.

Hydrogenation of nitrobenzene: Hydrogenation reactions were performed under constant H_2 flow (0.674 $cm^3\ s^{-1}$) using a Schlenk line. In a typical experiment, 0.5 mol % of catalyst and nitrobenzene solution (2 mL, 0.1 M), and a stir bar were added to a scintillation vial (5.0 mL). The vial was then placed in an oil bath under Schlenk line at 30 ^oC with stirring rate of 600 rpm. The reaction was performed for 30 min and aliquots were collected by centrifugation (4000 rpm). 100 µL of aliquot, 100 µL of internal standard (0.1 M Nitrophenol solution), and 800 µL of ethanol were mixed in a GC vial. The reaction products were then analyzed using Agilent GC-MS 7890 A equipped with 5975 C mass selective detector, column HP-5 30 m X 0.25 mm X 0.25 um. The run started at 50 ^oC and was held at that temperature for 1 min, followed by a temperature ramp to 170 ^oC at a rate of 10 $^oC\ min^{-1}$. The temperature was then ramped to 300 ^oC at ramp rate of 10 $^oC\ min^{-1}$ and was held at that temperature for 1 min.

Characterization

Textural properties: Nitrogen sorption isotherms were obtained in a Micrometrics Tristar analyzer at -196^oC. Brunauer-Emmett-Teller (BET) and Barret-Joyner Halenda (BJH) methods

were used to calculate surface area and pore size distribution respectively. The samples were degassed under N_2 flow for 6 h at 100°C prior to the analysis.

Powder X-ray diffraction: Small- and wide-angle X-ray diffraction patterns were collected on a Bruker AXS D8 Discover powder diffractometer equipped with Cu Kα radiation source (40 kV, 44 mA) over the range of 1–10° (low angle) and 10-60° (wide angle) (2θ). The sample was scanned in 0.02 ° steps. Crystallite sizes were calculated using Scherrer's equation:

$$D = \frac{K\lambda}{\beta cos\theta}$$

Where K is the shape factor of the average crystallite with a value of 0.93.[43] λ is the wavelength of incoming X-rays (0.154 nm), β is the full width half-maximum, and Θ is the Bragg's angle. All the crystallite sizes were calculated using the reflection at 2Θ = 40 degrees.

Diffuse reflectance infrared Fourier transform spectroscopy (DRIFT): A Bruker vertex 80 FTIR spectrophotometer equipped with a HeNe laser and photovoltaic MCT detector and OPUS software was used to collect DRIFT spectra. The samples were vacuum dried at 100°C under Schlenk line for 24 h prior to analysis.

CHN elemental analysis: CHN elemental analysis was performed using a Perkin Elmer 2100 Series II analyzer using acetanilide as a calibration standard. The carbon materials were vacuum dried at 100°C under Schlenk line for 12 h prior to analysis. Triplicate runs for each sample were performed.

X-Ray photoelectron spectroscopy (XPS): XPS analysis was performed using a Kratos Amicus (ESCA 3400) system using standard - Al X-rays. The samples were prepared by deposition onto a double-sided-tape sample holder. All spectra were energy calibrated based on C 1*s* peak set at 284.6 eV.

Inductively coupled plasma optical emission spectroscopy (ICP-OES): A PerkinElmer Optima 2100 inductively coupled plasma optical emission spectrometer was used for quantification of palladium. 5.0 mg of carbon material was calcined in a box furnace at 500ºC for 6 h. The calcined material was then treated with 20 vol% aqua regia (10 mL) and ICP-OES was then performed. Three runs were performed on each material and an average was taken to calculate the wt% of palladium.

Transmission electron microscopy (TEM): TEM analysis was conducted using a FEI Tecnai G2 F20 field emission microscope operating at 200 kV. TEM samples were prepared by placing 2−3 drops of dilute ethanol suspensions onto lacey-carbon-coated copper grids. The particle size of supported palladium nanoparticle was determined by measuring the size of at least 60 palladium nanoparticles from the TEM images.

Results & Discussions

Table 1 shows the structural properties of N-OMCs and OMCs. All synthesized materials show type IV N_2 sorption isotherms that are characteristic of mesoporous materials. Surface area and pore volume increase as the carbonization temperature increases. The adsorption and desorption branches of some isotherms do not close. This sorption behavior is related to micropore formation at these carbonization temperatures.[44] The pore size of all OMC materials ranges between 2 to 4 nm. The low-angle powder XRD patterns of all OMC (Fig. 1B) and N-OMC (Fig. 1D) show a strong diffraction peak at 0.90 2θ º. Some additional weak diffraction peaks are also observed at 2θ = 1.4-1.6 º. These peaks are associated with (100), (110), and (200) reflections of 2D-hexagonal P*6mm* symmetry.[42]

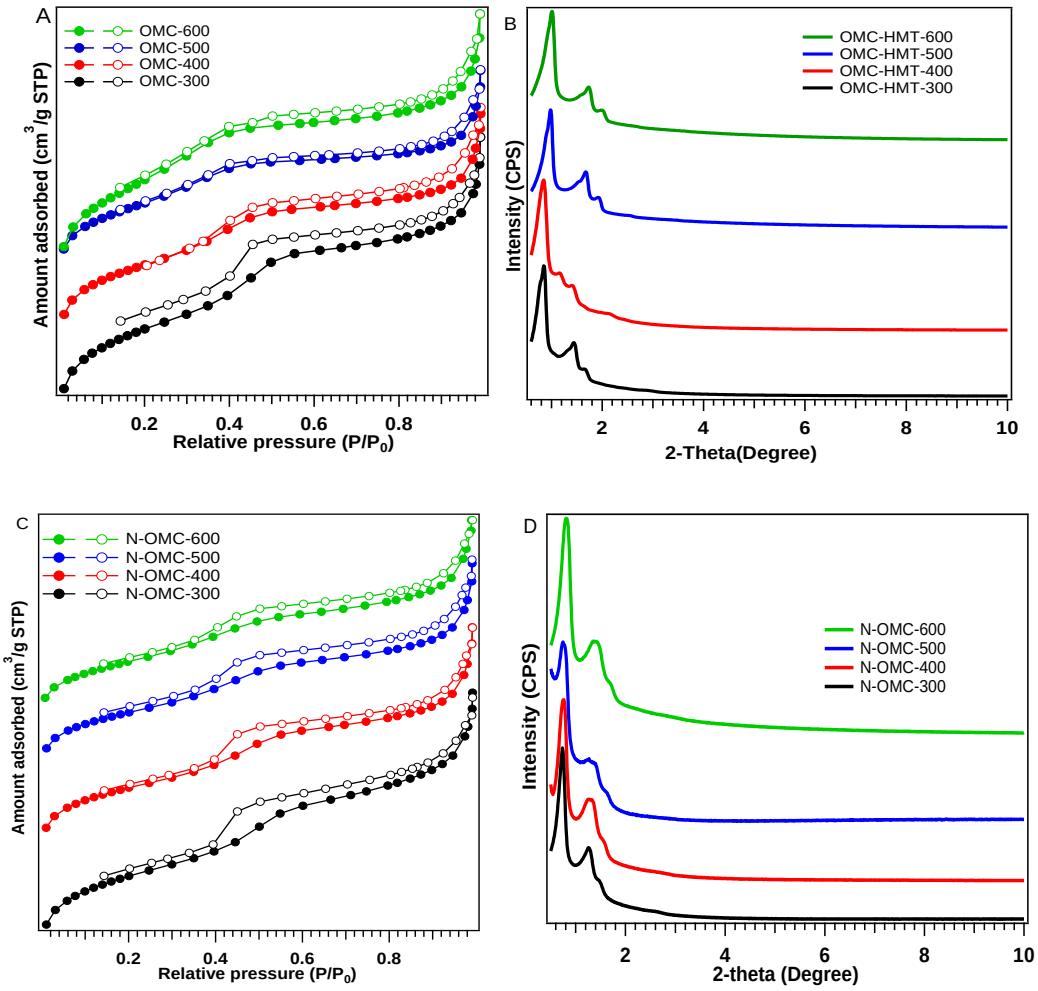

Figure 1. A) N_2 sorption isotherms and **B)** low-angle XRD patterns of OMC, and **C)** N_2 sorption isotherms and **D)** low-angle XRD patterns of N-OMC carbonized at 300, 400, 500, and 600 ^oC.

CHN elemental analysis was performed on OMC and N-OMC materials to study their composition. As shown in Table 1, N remains between 8 and 9% at carbonization temperatures 300 – 500 °C, and only seems to start dropping at 600 °C. This behavior is expected as nitrogen will be eliminated as a N_2, and NH_3 gases with increasing carbonization temperature.[35] A similar trend is also observed for %H and %O. The constant decrease in %H with carbonization temperature suggests increasing formation of the aromatic framework.

DRIFT spectra of OMC and N-OMC are shown in Figure 2. N-OMCs (figure 2B) carbonized at 300 and 400 ^oC present a band at 3400-3500 cm^{-1}, which may be related to N-H or O-H

stretching vibrations.[45] To the contrary, OMC does not show absorption in this region. Thus, the band at 3400-3500 cm^{-1} in N-OMC can be attributed to N-H bonds in the primary amine from

Table 1: Structural properties and elemental composition of OMC and N-OMC carbonized at various temperature. %O was calculated using equation 100- (%H + %C + %N).

Material	Surface Area ($m^2.g^{-1}$)	Pore size (nm)	Pore Volume ($cm^3.g^{-1}$)	% C	% N	% H	% O
OMC-300	458	3.5	0.36	73.2±0.4	1.37±0.08	4.25±0.43	19.3±0.28
OMC-400	524	3.1	0.36	74.7±0.5	1.23±0.07	3.74±0.27	18.1±0.45
OMC-500	607	2.8	0.38	89.0±0.5	1.35±0.07	2.81±0.02	6.81±0.53
OMC-600	837	2.6	0.50	91.4±0.3	2.80±0.11	1.19±0.06	4.61±0.41
N-OMC-300	461	3.5	0.41	72.9±0.9	8.27±0.15	3.97±0.09	14.9±1.08
N-OMC-400	506	3.5	0.39	78.0±0.4	8.93±0.07	3.07±0.02	10.0±0.47
N-OMC-500	531	3.5	0.39	81.7±0.6	8.48±0.19	2.60±0.28	7.85±0.62
N-OMC-600	523	3.3	0.37	82.1±0.8	7.09±0.11	1.83±0.15	9.54±0.82

the nitrogen-carbon precursor – 3-aminophenol. Upon increasing carbonization temperature to 400 ºC, N-H band gives a single peak attributing secondary amine entity such as pyrrolic N. The N-H band around 3400-3500 cm^{-1} disappeared at a carbonization temperature of 600 ºC. The disappearance of N-H band suggests pyridinic and quaternary nitrogen type of structure formation at higher temperatures. The strong absorptions around 1500-1700 cm^{-1} (figure 2B) are

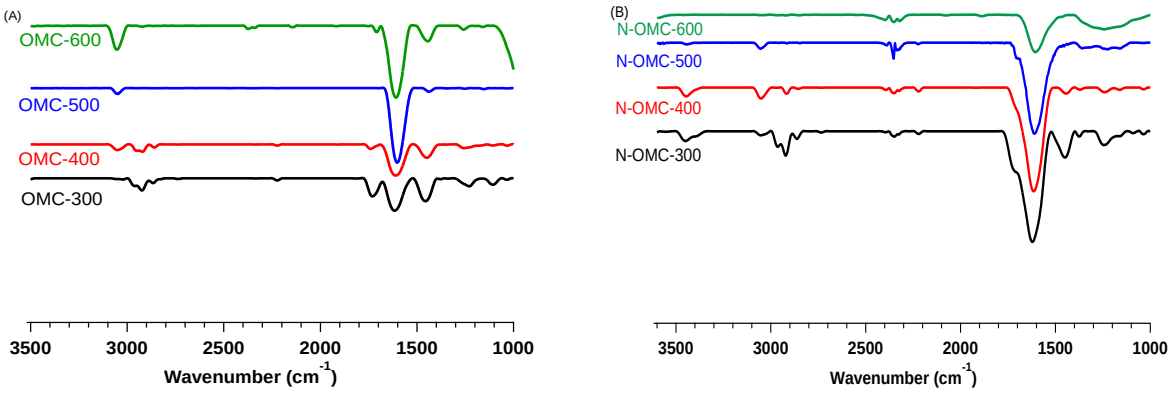

Figure 2: (A) DRIFT spectra of OMC and **(B)** DRIFT spectra of N-OMC carbonized at 300, 400, 500 and 600 ºC.

attributed to C=C, C=N, and -N-H(*w*) stretching vibrations.[46,47] A weak C-N stretching vibration (figure 2B) is observed at 1250 cm^{-1} in nitrogen-doped carbons carbonized at 300 and 400 ºC suggesting the presence of primary and secondary amine functionalities.46,[48] The band at 2800-3000 cm^{-1} (Figure 2A & B) shows presence of –C-H bond from aliphatic carbons while the bands between 3000-3200 cm^{-1} suggests presence of –C=C-H bond from aryl rings.[49] As the carbonization temperature increases, the peak for -C-H starts to disappear which is attributed to the formation of an aromatic framework in both carbon materials. The band at 1620 cm^{-1} (figure 2A) are ascribed to C=C and O-H stretching vibration of hydroxyl group from carbon precursor – resorcinol.[50] Additionally, a stretching band for C=O is observed around 1720 cm^{-1} for OMC carbonized at 300 and 400 ºC suggesting the presence of formaldehyde.

XPS analysis was performed to analyze the chemical environment of nitrogen and carbon species in OMC and N-OMC materials at carbonization temperatures between 300 and 500 ºC. The N1s peaks in N-OMC materials can be deconvoluted into four different components: amine (399.4 eV), pyridinic (398.4 eV), pyrrolic (400 eV), and quaternary (401.1eV) nitrogen.[51,52] N1s XPS spectra of these materials showed dominance in pyridinic and pyrrolic groups as carbonization temperature increases from 300 to 500 ºC.[49,53] The formation of pyridinic and pyrrolic nitrogen functionalities can be attributed to formation of N radicals with increasing carbonization temperature. These radicals can then attack the carbon to form functionalities such as pyrrole, pyridinic N, and nitrogen oxide.[22] C1s XPS spectra of these materials can be deconvoluted into many different components, including graphitic C (284.6 eV), C-N (285.6 eV), C=N (287.3 eV), and π-π* shake-up satellite peaks (290.2 eV).[54] C-N and C=N functionalities suggests the presence of amine, pyrrolic and pyridinic types of components in these materials.[51] A similar behavior was also observed via FTIR and CHN elemental analysis.

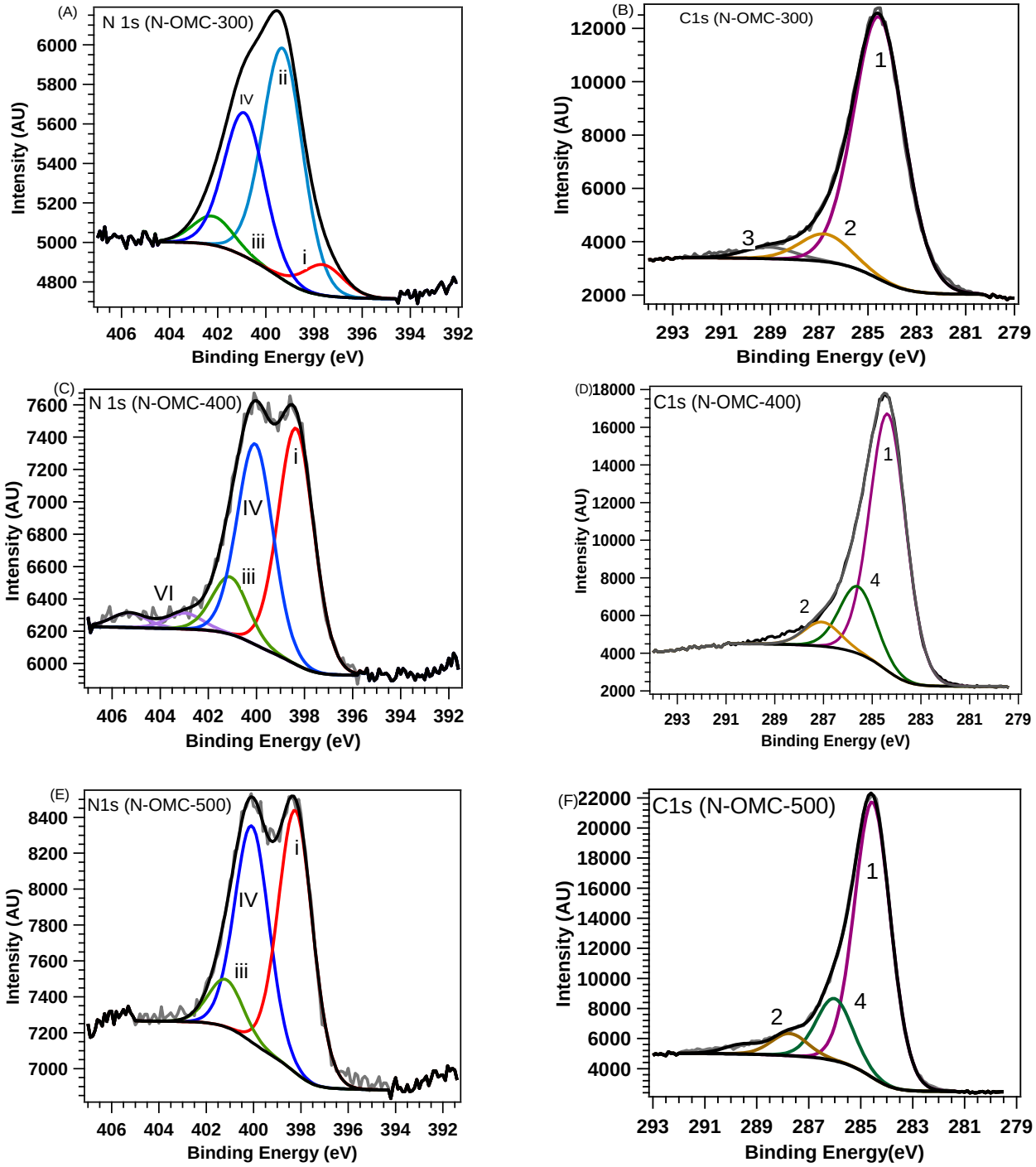

Figure 3: N1s and C1s XPS Spectra of N-OMC-300,400, and 500 °C. The colored lines in N1s XPS spectra for N-OMC represent: **(i)** pyridinic N (red), **(ii)** amine group (teal), **(iii)** quaternary N (green), **(iv)** pyrrolic N (blue) and **(vi)** pyridinic nitrogen oxide (light purple). The colored lines in C1s XPS spectra for N-OMC represent: **(1)** graphitic C (dark purple), **(2)** C=N bonds (mustard), **(3)** satellite peaks (grey), and **(4)** C-N (dark green).

Raman spectroscopy was employed to characterize structural defects and degree of graphitization in both carbon materials (Figure 4). Both materials exhibited two Raman bands located at 1340 cm^{-1} (D-band) and 1572 cm^{-1} (G-Band), respectively. The D-band corresponds to A_{1g} in plane vibrational mode, which is related to defects in the graphitic structure.[55,56,57] While, the G-band is indication of E_{2g} in plane vibration of sp^2 bonded carbons, suggesting the graphitic structure of the carbon material.[51,52,53] Table 2 shows ratio of the intensity of the D band to that of the G band (I_D/I_G). I_D/I_G was higher for N-OMC than that of OMC carbonized at the same temperatures, indicating that the degree of graphitization decreases upon incorporating nitrogen entities within the carbon framework.

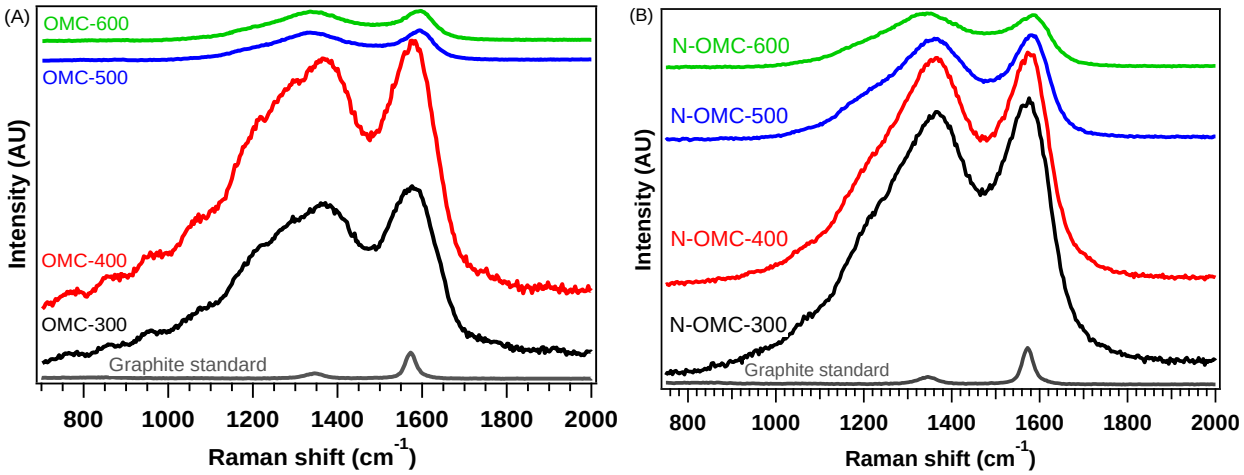

Figure 4: Raman spectra of (A) OMC and (B) N-OMC carbonized at 300, 400, 500, and 600 ºC.

Table 2: Intensity ratios from Raman spectra of OMC and N-OMC carbonized at 300,400, 500, and 600 ºC.

Material	I_D/I_G	Material	I_D/I_G
Graphite standard	0.21±0.04	***Graphite standard***	0.21±0.04
N-OMC-300	0.90±0.10	**OMC-300**	0.84±0.06
N-OMC-400	1.00±0.10	**OMC-400**	0.81±0.01
N-OMC-500	1.06±0.04	**OMC-500**	0.97±0.01
N-OMC-600	1.23±0.04	**OMC-600**	0.94±0.03

After successful characterization of these carbon materials, they were impregnated with $Pd(NO_3)_2{\cdot}2H_2O$. The materials were then reduced using $NaBH_4$/EtOH solution. The N_2 sorption

isotherms of Pd-OMCs and Pd-N-OMCs showed type IV behavior, indicating the mesoporous character was preserved after metal formation. The surface areas of these materials are 20% smaller than the original OMCs and N-OMCs. This behavior is likely to be caused by sintering

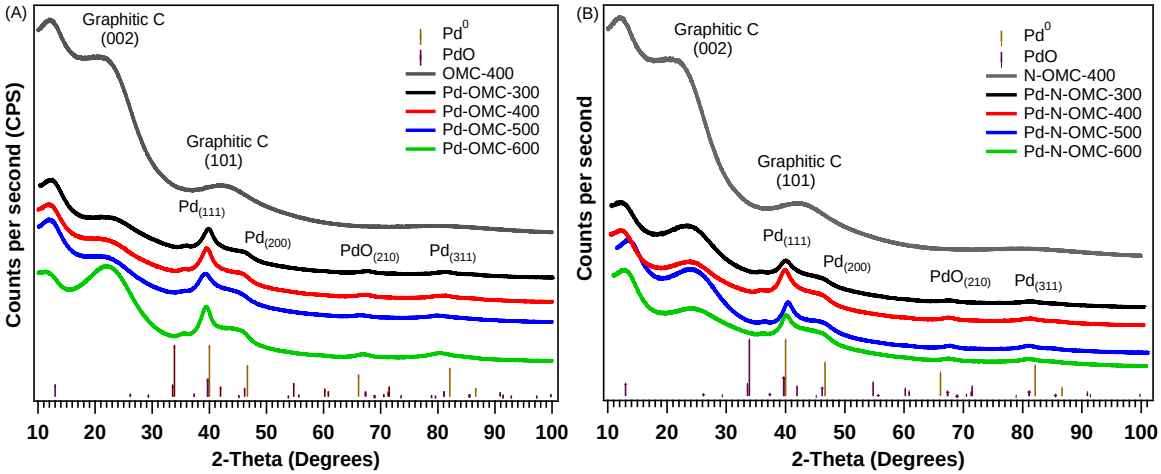

Figure 5: XRD patterns of (A) Pd-OMC and (B) Pd-N-OMC carbonized at 300, 400, 500, and 600 °C.

Table 3: Structural properties of Pd supported OMC and N-OMC. [a]Crystallite size was calculated using XRD peak at $2\Theta = 40.1^{o}$. [b]Wt% of Pd was measured by ICP-OES.

Material	Surface Area (m^2/g)	Pore Size (nm)	Pore Volume (cm^3/g)	Crystallite size (nm)[a]	Pd Wt%[b]
Pd-OMC-300	323	3.2	0.24	4.6	1.4±0.3
Pd-OMC-400	457	2.9	0.29	4.4	1.7±0.2
Pd-OMC-500	380	2.6	0.27	4.1	1.8±0.04
Pd-OMC-600	405	2.7, 3.9	0.26	4.5	1.3±0.03
Pd-N-OMC-300	237	3.5	0.23	4.3	1.8±0.1
Pd-N-OMC-400	313	3.2	0.26	4.6	1.9±0.2
Pd-N-OMC-500	362	3.2	0.30	4.5	1.6±0.1
Pd-N-OMC-600	125	3.1	0.15	4.5	1.7±0.2

of metal that leads to pore filling or blocking. Figure 5 shows the wide-angle XRD patterns of OMC and N-OMC materials. Both materials show two notable peaks at 23.2 and 42.7 $2\Theta^{o}$ which correspond to (002) and (101) reflections from carbon supports, respectively A strong diffraction peak for metallic Pd is observed at 40.1 $2\Theta^{o}$ followed by weak diffraction peaks at 35.6, 46.6,

67.3, and 81.3 $2\Theta^{o}$.[58] The crystallite sizes of both materials range between 4.0 to 4.6 nm which is on the same order of magnitude as the pore width suggesting that most of palladium is incorporated within the mesopores of the OMC materials. The XRD patterns of Pd in OMC and N-OMC do not show significant differences between the materials.

XPS analysis was performed to scrutinize the electronic state of palladium. XPS analysis of Pd 3d suggests that palladium species are present as Pd^{0} and Pd^{2+} electronic states. Metallic palladium is the dominant phase observed on the surface of Pd-OMC while Pd^{2+} is the dominant phase on the surface of Pd-N-OMC. The binding energies of Pd^{0} and Pd^{2+} are shifted to higher values in Pd-OMC (341.7 eV, 344.3 eV) compared to those in Pd-N-OMC. (341.4 eV, 344.1 eV) Similar trend was also observed by Lee and co-workers.[59] Lee and co-workers observed that Pd^{2+} is likely to interact with sp^{2} orbitals of nitrogen atoms. Due to such strong interactions between nitrogen atoms and Pd^{2+} species, palladium will be harder to reduce to its metalic state and better dispersion can be attained.[59] Ombaka and co-workers suggested the possible interactions between Pd nanoparticles and nitrogen functionalities in N-doped carbon nanotubes.[60] They proposed that pyrrolic nitrogen functionalities tend to covalently bind with Pd^{2+} species, while lone electron pairs from pyridinic N tend to coordinate with vacant sites of Pd^{2+} (Scheme 1).[61] These interactions may be responsible for preventing the reduction to Pd^{0}.

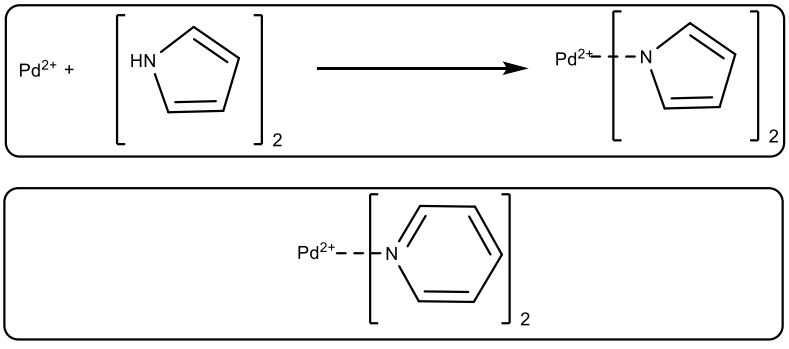

Scheme 1: Possible interactions between pyrrolic and pyridinic N functionalities and Pd nanoparticles.[60,61]

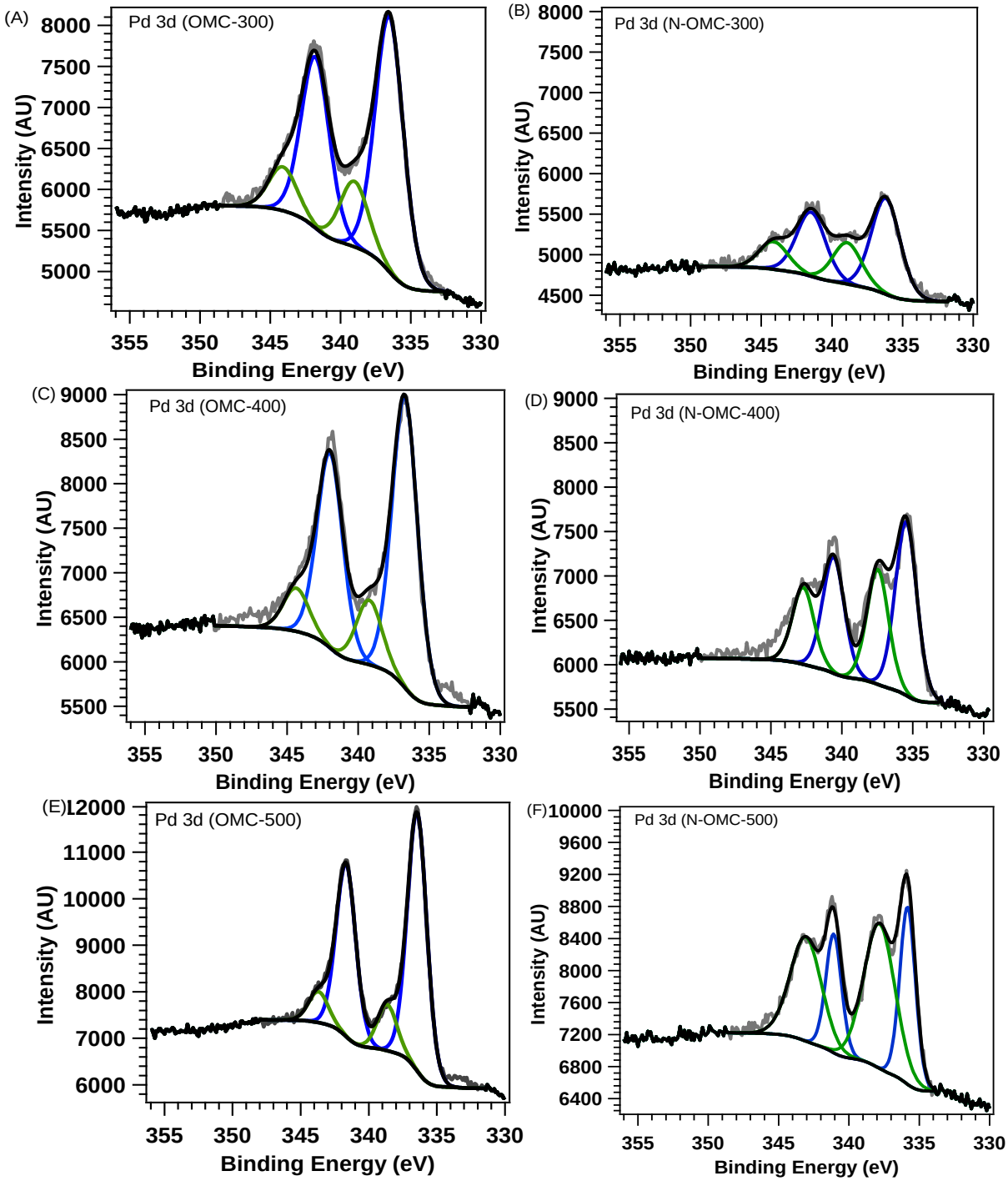

Figure 6: Pd 3d XPS spectra of Pd-OMC and Pd-N-OMC. Blue line represents metalic palladium (Pd^0), Green line represents Pd^{2+} species

As can be seen in Figures 7 and 8, palladium nanoparticles are better dispersed in Pd-N-OMC in than in Pd-OMC. N1s XPS analysis (Figure 3) showed the formation of pyridinc and pyrrolic N

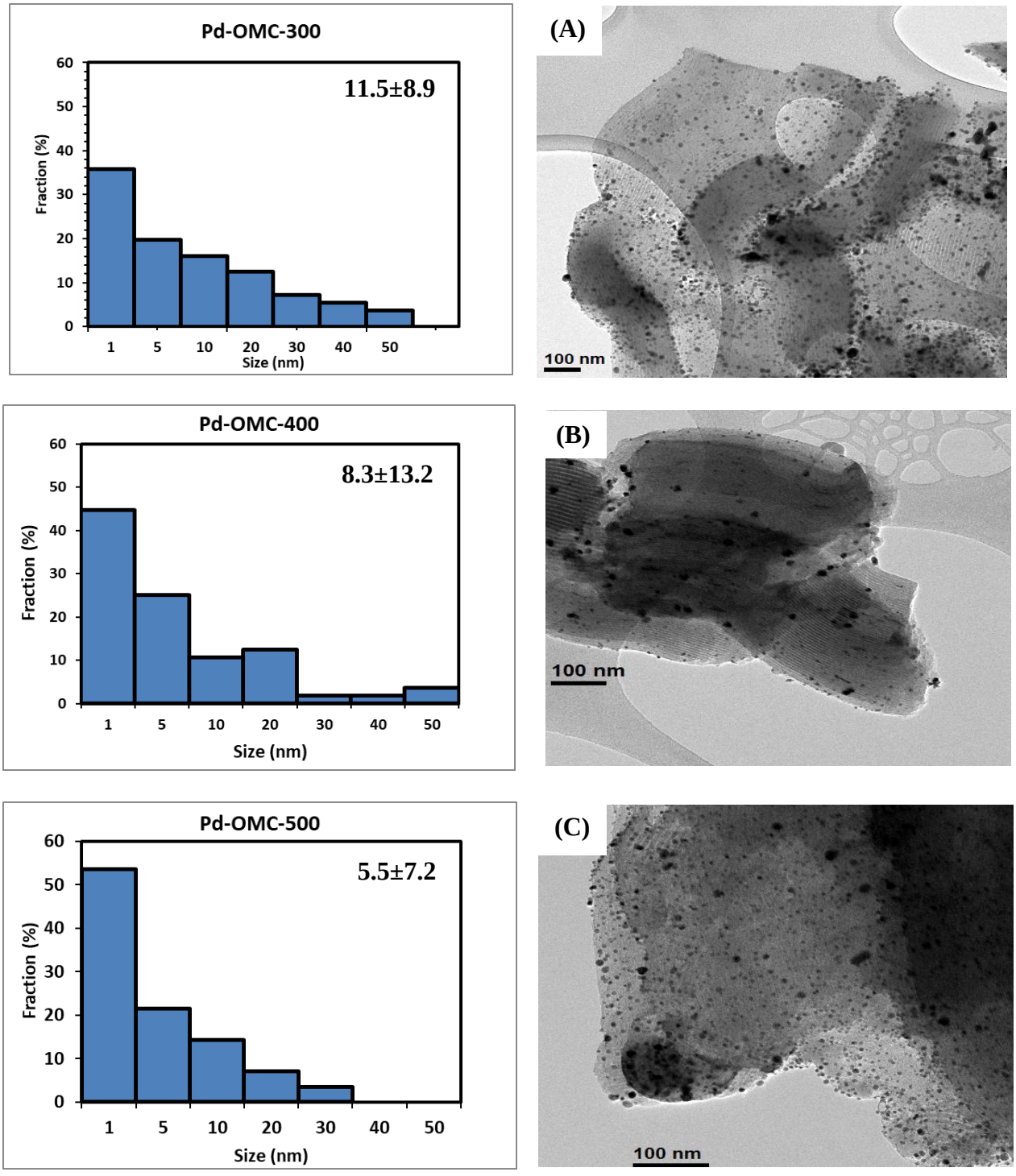

Figure 7: TEM images and Pd particle size histograms of Pd-OMC carbonized at **(A)** 300, **(B)** 400, and **(C)** 500 ºC. (Particle size average and standard deviations in nm indicated in the top right corner of the histograms).

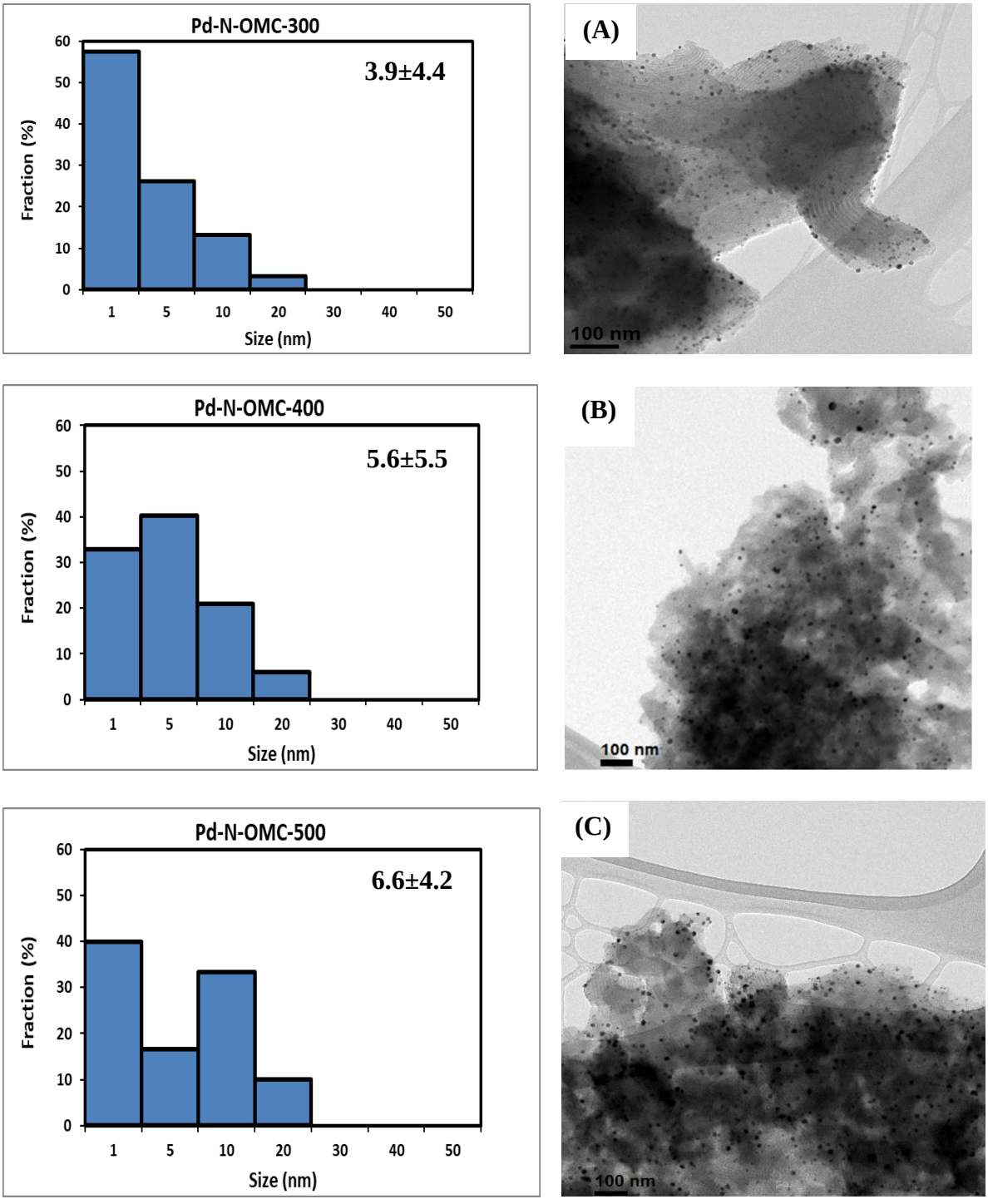

Figure 8: TEM images and Pd particle size histograms of Pd-N-OMC carbonized at **(A)** 300, **(B)** 400, and **(C)** 500 ^{o}C. (Particle size average and standard deviations in nm indicated in the top right corner of the histograms).

structures at higher carbonization temperatures. Better dispersion of palladium nanoparticles can be ascribed to strong interactions between nitrogen functionalities and palladium species. TEM images of Pd-OMC (Figure 7) and Pd-N-OMC (Figure 8) showed that most of the palladium particle size ranges between 1 and 20 nm. As shown in Figure 7a and b, Pd-OMC carbonized at 300 and 400 ^{o}C showed agglomeration of palladium nanoparticles (particle size = 30-50 nm) compared to that of Pd-N-OMC carbonized at the same temperature. Additionally, higher dispersion and smaller particle size of palladium is observed in Pd-N-OMC-300 and 400 compared to that of Pd-N-OMC-500. This behavior is ascribed to presence of nitrogen entities such as amine group, pyrrolic, and pyridinic nitrogen in Pd-N-OMC-300 and 400.

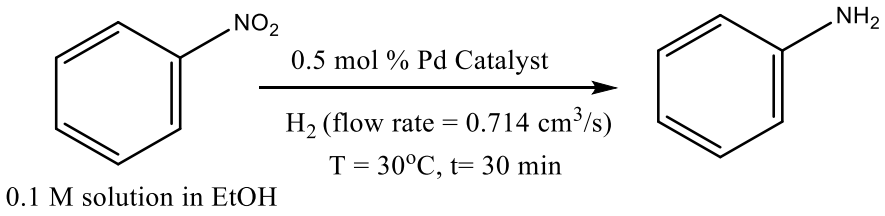

Scheme 2: Catalytic hydrogenation of nitrobenzene to aniline using ethanol as a solvent.

Pd-OMC and Pd-N-OMC materials were then evaluated as catalysts to study the influence of nitrogen doping on the hydrogenation of nitrobenzene (Figure 9). Aniline is produced as a major product of the reaction. Pd-OMC-500 showed higher production of aniline compared to Pd-OMC-300 and 400. The Pd size distributions of OMC (Figure 7) indicated smaller metal nanoparticle sizes (5.5±7.2) in the material carbonized at 500, suggesting that the lower catalytic activity of Pd-OMC-300 and 400 materials may be due to nanoparticle sintering. Donoeva and co-workers also observed that while Au nanoparticles supported in graphite and O-modified graphite underwent significant Ostwald ripening, functionalization of the material with nitrogen

inhibited nanoparticle sintering.[62] They attributed this difference in sintering behavior to enahnced interaction of the metal with N-functionalities in the carbon material.

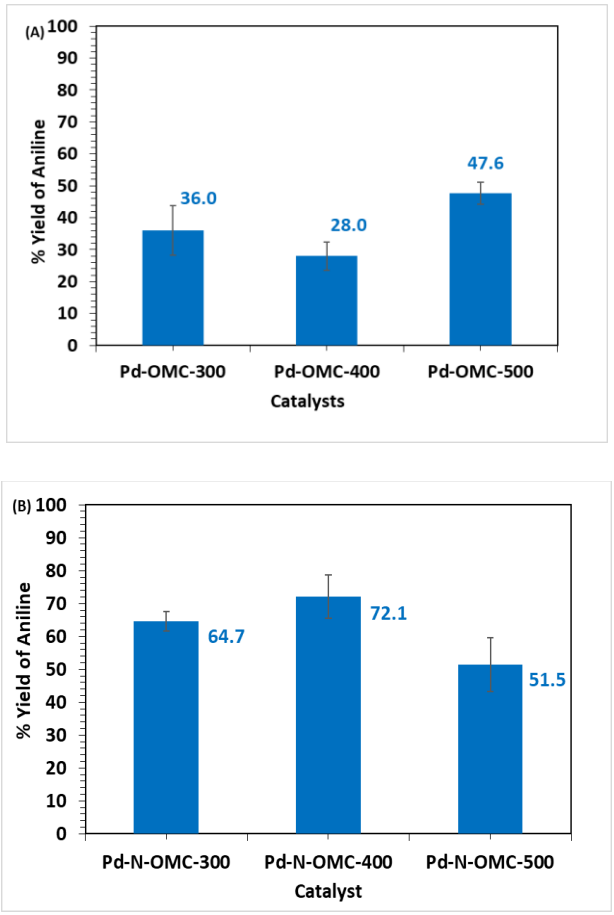

Figure 9: Catalytic hydrogenation of nitrobenzene using (A) Pd-OMC and (B) Pd-N-OMC carbonized at 300, 400, and 500 ^{o}C

Pd-N-OMC materials exhibited higher activity compared to Pd-OMC materials. The difference is likely due to a combination of factors including better dispersion of the metal as suggested from TEM imaging (Figures 7 and 8), and the capacity of N to donate electrons to the supported metal. The nitrogen functionalities on carbon support act as a lewis base. Among three dominant nitrogen functionalities present in N-OMC materials, pyridine is the most basic in nature compared to aniline and pyrrole. This would explain the slightly higher activity of Pd-N-OMC-400 compared to Pd-N-OMC-300 based on the higher pyridinc N content of the former (Figure

3), the activity of the pyridinic-N rich Pd-N-OMC-500 is the lowest of the three doped materials. Due to higher basicity of pyridine N, it is a better electron donor than N in pyrrole and amine (aniline) groups, and can therefore affect more efficiently the electronic properties of Pd nanoparticles resulting in enhancement of the catalytic activity. Ombaka and co-workers also reported a similar behavior. They observed that the presence of pyridine-Pd complexes in carbon materials enhances catalytic acitivity and selectivity for hydrogenation of nitroarenes compared to pyrrole-Pd complexes.[61] The small decrease in catalytic activity observed for Pd-N-OMC-500 could be due to a slightly larger particle size as observed from TEM (Figure 8) and a higher Pd^{2+} content as evidenced by XPS analysis (Figure 6).

Conclusions

In summary, N-OMCs with high surface area and large pore volume have been successfully synthesized via condensation between 3-aminophenol and formaldehyde. Using this procedure, 6-8 wt % of nitrogen and direct incorporation of nitrogen functionalities were achieved. At higher carbonization temperatures, N-OMCs tend to form pyrrolic and pyridinic types of nitrogen functionalities within the carbon framework. Presence of such nitrogen functionalities likely acted as coordination ligands to prevent sintering of Pd nanoparticles resulting in better dispersion as observed in TEM images. Strong metal-support interactions between palladium and nitrogen-functionality and electronic effects of the N-dopant resulted in better catalytic activity for hydrogenation of nitrobenzene using Pd-N-OMC compared to Pd-OMC.

References

[1] Zang, W.; Li, G.; Wang, L.; Zhang, X. Catalytic Hydrogenation by Noble-Metal Nanocrystals with Well-Defined Facets: A Review, *Catal. Sci. Technol.*, **2015**, *5*, 2532–2553.

[2] Ono, N. Conversion of Nitro Compounds into Other Compounds. *The Nitro Groups in Organic Synthesis. Wiley-VCH: New York*, **2001**, 159-177.

[3] Goldschmidt; M.; Fung, D.; Grant R; White; J.; Brown, T. New Aniline Blue Dye Medium for Rapid Identification and Isolation of Candida Albicans, *J. Clin. Microbiol.*, **1991**, *29*, 1095–1099.

[4] Rickert, D. Toxicity of Nitroaromatic Compounds. Washington: Hemisphere Toxicon, **1985**, 1-121.

[5] Downing, R. S.; Kunkeler, P. J.; Bekkum; V. Catalytic Synthesis of Aromatic Amines, *Catal. Today*, **1997**, *37*, 121–136.

[6] Smith, A.; Whyman, R. Review of Methods for the Catalytic Hydrogenation of Carboxamides. *Chem. Rev.*, **2014**, *114*, 5477–5510.

[7] Nishimura, S. Handbook of Heterogeneous Catalytic Hydrogenation for Organic Synthesis. *John Wiley & Sons*, **2001**.

[8] Rylander, P. Catalytic Hydrogenation in Organic Syntheses. *Academic Press*, **1979**.

[9] Bouchenafa-Saı¨b, N.; Grange, P.; Verhasselt, P.; Addoun, F.; Dubois, V. Effect of Oxidant Treatment of Date Pit Active Carbons used as Pd Supports in Catalytic Hydrogenation of Nitrobenzene, *App. Cat. A*, **2005,** *286*, 167–174.

[10] Gelder, E.; Jackson, D.; Lok, M. A Study of Nitrobenzene Hydrogenation Over Palladium/Carbon Catalysts, *Catal. Lett.* **2002**, *84*, *3*, 205-208.

[11] Pikna, L.; Heželová, M.; Demčáková, S.; Smrčová, M.; Plešingerová, B.; Štefanko, M.; Turáková, M.; Králik, M.; Puliš, P.; Lehocký, P. Effect of Support on Activity of Palladium Catalysts in Nitrobenzene Hydrogenation, *Chem. Pap.*, **2014**, *68*, 591-598.

[12] Turáková, M.; Králik, M.; Lehocký, P.; Pikna, Ľ.; Smrčová, M.; Remeteiová, D.; Hudák, A. Influence of Preparation Method and Palladium Content on Pd/C Catalysts Activity in the Liquid Phase Hydrogenation of Nitrobenzene to Aniline, *Appl. Catal. Gen.*, **2014**, *476*, 103–112.

[13] Li, C.; Yu, Z.; Yao, K.; Ji, S.; Liang, J. Nitrobenzene Hydrogenation with Carbon Nanotube-Supported Platinum Catalyst under Mild Conditions, *J. Mol. Catal. Chem.*, **2005**, *226*, 101–105.

[14] Takasaki, M.; Motoyama, Y.; Higashi, K.; Yoon, S.-H.; Mochida, I.; Nagashima, H. Chemo selective Hydrogenation of Nitroarenes with Carbon Nanofiber-Supported Platinum and Palladium Nanoparticles, *Org. Lett.*, **2008**, *10*, 1601–1604.

[15] Xu, Q.; Yazawa, T. Nanoporous Materials Synthesis and Applications, *taylor&francis*, **2013,** 1-121.

[16] Lu, A.; Schüth, F. Nanocasting: A Versatile Strategy for Creating Nanostructured Porous Materials, *Adv. Mater*., **2006**, *18*, 1793–1805.

[17] Liang, C.; Li, Z.; Dai, S. Mesoporous Carbon Materials: Synthesis and modification, *Ange. Chemie. Int. Ed.* **2008**, *47*, 3696–3717.

[18] Shen, W.; Fan, W. Nitrogen-Containing Porous Carbons: Synthesis and Application, *J. Mater. Chem. A*, **2013**, *1*, 999-1013.

[19] Zhao, L.; Baccile, N.; Gross, N.; Zhang, Y.; Wei, W.; Sun, Y.; Antonietti, M.; Titirici, M. Sustainable Nitrogen-doped Carbonaceous Materials from Biomass Derivatives, *Carbon*, **2010**, *48*, 3778 – 3787.

[20] Zhao, L.; Fan, L.; Zhou, M.; Guan, H.; Qiao, S.; Antonietti, M.; Titirici, M. Nitrogen-Containing Hydrothermal Carbons with Superior Performance in Supercapacitors, *Adv. Mater.* **2010**, *22*, 5202-5206.

[21] Boehm, H.; Mair, G.; Stoehr, T.; Rincon, D.; Ana, R.; Tereczki, B. Carbon as a Catalyst in Oxidation Reactions and Hydrogen Halide Elimination Reactions, *Fuel*, **1984**, *63*, *8*, 1061-1063.

[22] Zhao, A.; Masa, J.; Schuhmann, W.; Xia, W. Activation and Stabilization of Nitrogen-doped Carbon Nanotubes as Electrocatalysts in the Oxygen Reduction Reaction at Strongly Alkaline Conditions, *J. Phys. Chem. C*, **2013,** *117*, 24283-24291.

[23] Shin, D.; Jeong, B.; Mun, B.; Jeon, H.; Shin, H.; Baik, J.; Lee, J. On the Origin of Electrocatalytic Oxygen Reduction Reaction on Electrospun Nitrogen−Carbon Species, *J. Phys. Chem. C*, **2013,** *117*, 11619-11624.

[24] Jagdeesh, R.; Stemmler, T.; Sarkus, A.; Junge, H.; Junge, K.; Beller, M. Hydrogenation using Iron-Oxide Based Nanocatalysts for the Synthesis of Amines, *Nature*, **2015**, *10*, *4*, 548-557.

[25] Wang, X.; Lee, J. S.; Zhu, Q.; Liu, J.; Wang, Y.; Dai, S. Ammonia-Treated Ordered Mesoporous Carbons as Catalytic Materials for Oxygen Reduction Reaction, *Chem. Mat.*, **2010,** *22*, *7*, 2178-2180.

[26] Lin, Z.; Waller, G.; Liu, Y.; Liu, M.; Wong, C. Facile Synthesis of Nitrogen-Doped Graphene via Pyrolysis of Graphene Oxide and Urea, and its Electrocatalytic Activity Toward the Oxygen-Reduction Reaction, *Adv. Energy Mater.*, **2012**, *2*, 884–888.

[27] Rivera-Utrilla, J.; Sánchez-Polo, M.; Gómez-Serrano, V.; Alvarez, P.; Alvim-Ferraz, M.; Dias, J. Activated Carbon Modifications to Enhance its Water Treatment Applications. An Overview, *J. Hazard. Mater.*, **2011**, *187*, 1-3.

[28] Hou, Z.; Terakura, K., Effect of Nitrogen Doping on the Migration of the Carbon Adatom and Monovacancy in Graphene. *J. of Phys. Chem. C*, **2015,** *119*, *9*, 4922-4933.

[29] Xia, Y.; Mokaya, R., Generalized and Facile Synthesis Approach to N-Doped Highly Graphitic Mesoporous Carbon Materials. *Chem. of Mat.*, **2005,** *17*, *6*, 1553-1560.

[30] Marjanovíc, G.; Pašti, I.; Mentus, S. One-Dimensional Nitrogen-Containing Carbon Nanostructures, *Prog. Mater. Sci.*, **2015**, *69*, 61–182.

[31] Martin-Hopkins, M.; Gilpin, R.; Jaroniec, M., Studies of the Surface Heterogeneity of Chemically Modified Porous Carbons by Gas-Solid Chromatography. *J. of Chromatogr. Sci.*, **1991,** *29*, *4*, 147-152.

[32] Lu,A.; Kiefer, A.; Schmidt, W.; Schüth, F. Synthesis of Polyacrylonitrile-Based Ordered Mesoporous Carbon with Tunable Pore Structures, *Chem. Mater.*, **2004**, *16*, 100-103.

[33] Vinu, A.; Anandan, S.; Anand, C.; Srinivasu, P.; Ariga, K.; Mori, T.; Fabrication of Partially Graphitic Three-Dimensional Nitrogen-Doped Mesoporous Carbon using Polyaniline Nanocomposite Through Nanotemplating Method, *Micro. Meso. Mat.*, **2008**, *109*, 398-404.

[34] Yang, C.; Weidenthaler, C.; Spliethoff, B.; Mayanna, M.; Schüth, F. Facile Template Synthesis of Ordered Mesoporous Carbon with Polypyrrole as Carbon Precursor, *Chem. Mater.*, **2005**, *17*, *2*, 355-358.

[35] Iraudet, S.; Zhu, Z.; Yao, X.; Lu, Z. Ordered Mesoporous Carbons Enriched with Nitrogen: Application to Hydrogen Storage, *J. Phys. Chem. C*, **2010**, *114*, *18*, 8639-8645.

[36] Feng, C.; Li, H.; Wan, Y. Fabrication of N-doped Highly Ordered Mesoporous Polymers and Carbons. *J. Nanosci. Nanotechnol.*, **2009**, *9*, *2*, 1558-1563.

[37] Yang, J.; Zhai, Y.; Deng, Y.; Gu, D.; Li, Q.; Wu, Q.; Huang, Y.; Tu, B.; Zhao, D. Direct Triblock-Copylmer-Templating Synthesis of Ordered Nitrogen-Containing Mesoporous Polymers, *J. of Colloid Interface Sci.*, **2010**, *342*, *2*, 579-585.

[38] Yu, J.; Guo, M.; Muhammad, F.; Wang, A.; Yu, G.; Ma, H. Zhu, G. Simple Fabrication of an Ordered Nitrogen-doped Mesoporous Carbon with Resorcinol-Melamine-Formaldehyde Resin, *Carbon*, **2014**, 502-514.

[39] Yu, J.; Guo, M.; Muhammad, F.; Wang, A.; Zhang, F.; Li, Q.; Zhu, G. One-Pot Synthesis of Highly Ordered Nitrogen-Containing Mesoporous Carbon with Resorcinol–Urea–Formaldehyde Resin for CO_2 Capture, *Micro. and Meso. Mat.*, **2014**, *190*, 117-127.

[40] Wang, J.; Liu, H.; Gu, X.; Wang, H.; Sheng Su, D. Synthesis of Nitrogen-Containing Ordered Mesoporous Carbon as a Metal-Free Catalyst for Selective Oxidation of Ethylbenzene, *Chem. Commun.*, **2014**, *50*, 9182 -9184.

[41] Shen, G.; Sun, X.; Zhang, H.; Lium H.; Zhang, J.; Meka, A.; Zhuo, L.; Yu, C. Nitrogen-doped Ordered Mesoporous Carbon Single Crystals: Aqueous Organic-Organic Self-Assembly and Superior Supercapacitor Performance, *J. Mater. Chem. A.*, **2015**, *3*, 24041-24048.

[42] Liu, D.; Lei, J.; Guo, L.; Qu, D.; Li, Y.; Su, B. One-Pot Aqueous Route to Synthesize Highly Ordered Cubic and Hexagonal Mesoporous Carbons from Resorcinol and Hexamine, *Carbon*, **2012**, *50*, 476-487.

[43] Patterson, A. The Scherrer Formula for X-ray Particle Size Determination, *Phys. Rev.*, **1939**, *56*, 978-982.

[44] Meng, Y.; Gu, D.; Zhang, F.; Shi, Y.; Cheng, L.; Feng, D.; A Family of Highly Ordered Mesoporous Polymer Resin and Carbon Structures from Organic–Organic Self-Assembly. *Chem Mater*, **2006**, *18, 18*, 4447–4464.

[45] Katsoulidis, A.; Kanatzidis, M. Phloroglucinol Based Microporous Polymeric Organic Frameworks with −OH Functional Groups and High CO_2 Capture Capacity, *Chem. Mater.*, **2011**, *23*, 1818-1824.

[46] Li, M.; Xue, J. Integrated Synthesis of Nitrogen-Doped Mesoporous Carbon from Melamine Resins with Superior Performance in Supercapacitors, *J. Phys. Chem.* C, **2014**, *118*, 2507−2517.

[47] Kim, Y.; Kim, M.; Yun, C.; Chang, J.; Park, C.; Inagaki, M. Comparative Study of Carbon dioxide and Nitrogen Atmospheric Effects on the Chemical Structure Changes during Pyrolysis of Phenol–Formaldehyde Spheres, J. Colloid Interface Sci., **2004**, *274*, 555.

[48]Kharlamov, A.; Bondarenko, M.; Kharlamova, G.; Gubareni, N.; Fomenko, V. A New Method of Synthesis Carbon with Onion-like Structure with (10-13 %) Content of Nitrogen from Pyridine, *Uni. J. of Mat. Sci.*, **2013,** *1*, *2*, 78-86.

[49] Biniak, S.; Szymanski, G.; Siedlewski, J.; Swiatkowski, A. The Characterization of Activated Carbons with Oxygen and Nitrogen Surface Groups, *carbon*, **1997**, *35*, *12*, 1799-1810.

[50] Cao, F.; Chen, J.; Ni, M.; Song, H.; Xiao, G.; Wu, W.; Gao, X.; Xen, K. Adsorption of NO on Ordered Mesoporous Carbon and its Improvement by Cerium, *RSC. Adv.*, **2014**, *4*, 16281-16289.

[51] Wang, X.; Liu, C.; Neff, D.; Fulvio, P.; Mayes, R.; Zhamu, A.; Fang, Q.; Chen, G.; Meyer, H.; Jang. B.; Dai, S. Nitrogen-Enriched Ordered Mesoporous Carbons Through Direct Pyrolysis in Ammonia with Enhanced Capacitive Performance, *J. Mater. Chem. A*, **2013**, *1*, 7920-7926.

[52] Kundu, S.; Xia, W.; Busser, W.; Becker, M.; Schmidt, D.; Havenith, M.; Muhler, M. The Formation of Nitrogen-Containing Functional Groups on Carbon Nanotube Surfaces: A Quantitative XPS and TPD Study, *Phys. Chem. Chem. Phys.*, **2010**, *12*, *17*, 4351-4359.

[53] Shao, Y.; Zhang, S.; Engelhard, M. H.; Li, G.; Shao, G.; Wang, Y.; Liu, J.; Aksay, I. A.; Lin, Y., Nitrogen-doped Graphene and its Electrochemical Applications, *J. of Mat. Chem.*, **2010,** *20*, *35*, 7491-7496.

[54] Park, M.; Ryu, J.; Kim, Y.; Cho, J. Corn Protein-derived Nitrogen Doped Carbon Materials with Oxygen-rich Functional Groups: A Highly Efficient Electrocatalyst for all-Vanadium Redox Flow Batteries, *Energy Environ. Sci.*, **2014**, *7*, 3727-3735.

[55] Alessandro, H.; Monteverde, V.; Band, S.; Specchia, S.; Zhang, L.; Zhang, J. Non-noble Fe-N_x Electrocatalysts Supported on the Reduced Graphene Oxide for Oxygen Reduction Reaction, *Carbon*, **2014**, *76*, 386-400.

[56] Shen, Z.; Shao, L.; Chen, J.; Bao, W.; Wang, F.; Xia, X. Catalyst-Free Synthesis of Nitrogen-Doped Graphene via Thermal Annealing Graphite Oxide with Melamine and its Excellent Electrocatalysis, *Am. Chem. Soc. Nano.*, **2011**, *5*, *6*, 4350-4358.

[57] Cho, Y.; Kim, H.; Baik, S.; Myung, Y.; Jung, C.; Kim, C.; Park, J.; Kang, H. Selective Nitrogen-Doping Structure of Nanosize Graphitic Layers, *J. Phys. Chem. C*, **2011**, *115*, *9*, 3737-3744.

[58] Wang, J.; Liu, L; Chou, S.; Liu, H.; Wang, J. A 3D Porous Nitrogen-Doped Carbon-Nanofiber Supported Palladium Composites an Efficient Catalytic Cathode for Lithium-Oxygen Batteries, *J. Mater. Chem. A*, **2017**, *5*, 1642-1671.

[59] Lee, J.; Ryu, J.; Kim, J.; Nam, S.; Han, J.; Lim, T.; Gautam, S.; Chae, K.; Yoon, C. Carbon Dioxide Mediated, Reversible Chemical Hydrogen Storage using a Pd Nanocatalyst Supported no Mesoporous Graphitic Carbon Nitride, *J. Mater. Chem. A.*, **2014**, *2*, 9490-9495.

[60] Ombaka, L.; Ndu ngu, P.; Nyamori, V. Pyrrolic Nitrogen-Doped Carbon Nanotubes: Physicochemical Properties, Interactions with Pd and Their Role in the Selective Hydrogenation of Nitrobenzophenone, *RSC. Adv.*, **2015**, *5*, 109-122.

[61] Ombaka, L.; Ndu ngu, P.; Kibet, J.; Nyamori, V. The Effect of Pyridinic- and Pyrrolic-Nitrogen in Nitrogen-Doped Carbon Nanotubes Used as Support for Pd-Catalyzed Nitroarene Reduction: an Experimental and Theoretical study, *J. Mat. Sci.*, **2017**, *52*, 10751–10765.

[62] Donoeva, B.; Masoud, N.; Jongh, P. Carbon Support Surface Effects in the Gold-Catalyzed Oxidation of 5-Hydroxymethylfurfural, *ACS. Catal.*, **2017**, 4581-4591.

CHAPTER 3

FUNCTIONALIZED PERIODIC MESOPOROUS ORGANOSILICA: SYNTHESIS, AND CHARACTERIZATION

In this study, we report the synthesis and characterization of a series of functionalized periodic mesoporous organosilica (PMOs) materials containing an organosilane in addition to the organic bridging groups. The PMOs were prepared via surfactant templated acidic route using 1,4-bis(triethoxysilyl)benzene (BTEB) and bis(triethoxysilyl)ethane (BTEE) as the organosilica sources. Four different functional groups were introduced into PMO by condensation of the organosilica sources with organosilanes (3-(aminopropyl)trimethoxysilane (AP), 4-(triethoxysilyl)butyronitrile (BN), N-(2-aminoethyl)-3-aminopropyl-trimethoxysilane (AEAP), and 3-(triethoxysilyl)propyl succinic anhydride (PSA)).

Introduction

Ordered mesoporous silicas, first synthesized by Kresge and co-workers via surfactant-templated condensation of orthosilicates, have gained a lot of attention due to relevant properties such as high surface areas, large pore volumes and tunable pore sizes.[1] These materials have been extensively used in various applications like catalysis, sensing, chromatography, and drug delivery.[2,3,4] The scope of applications of these materials can further be widened by introducing organic groups on their surface. The incorporation of organic functionalities into mesoporous silica walls is usually performed by adding an organosilane either to the silica precursor during synthesis (co-condensation route) or to a pre-synthesized mesoporous silica (post-synthetic grafting).[5] An alternate approach for preparing mesoporous silica-based materials rich in organic functionalities is by using building blocks that contain simultaneously the silica and organic precursors. Periodic mesoporous organosilicas (PMO) belong to a class of organic-inorganic composites that have an organic bridging group incorporated within silica channel walls.[6,7,8] The

generic form of parent PMOs is $O_{1.5}Si\text{-}R\text{-}SiO_{1.5}$. The formula is based on stochiometric ratios between silicon and oxygen atoms. The form represents that three hydrolyzed silanol groups go through condensation reaction to form Si-O-Si bond so that every oxygen atom is shared between two silicon atoms.[6,7] As shown in Figure 1, PMO is synthesized via condensation between organosilane precursors in presence of SDA.

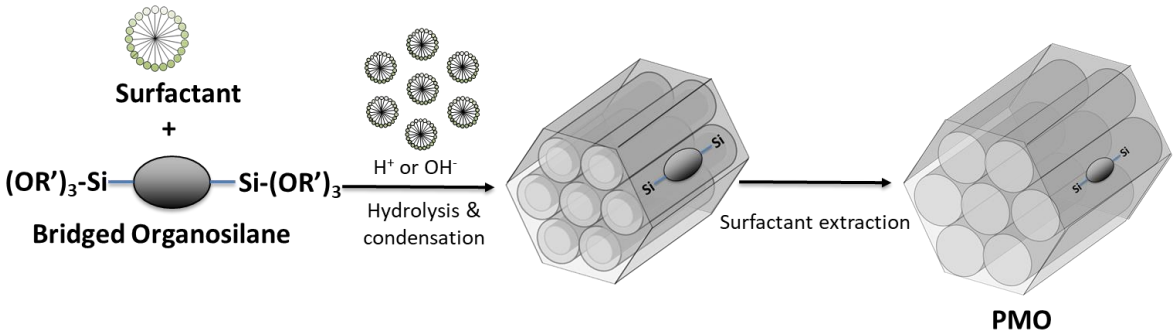

Figure 1: Schematic diagram of synthesis of periodic mesoporous organosilica (PMO)

In 1999, Ozin's group was the first one to synthesize PMOs followed by Stein and Inagaki groups.[9,10,11] Ozin and co-workers synthesized PMOs containing ethenylene bridging group (bis(triethoxysilyl)ethene) in presence of cationic surfactant under basic conditions. The support was then brominated to determine accessibility of ethenylene bridging group.[9] Stein and co-workers also synthesized ethylene and etheneylene bridged PMO using trimethylammonium bromide (CTAB) as SDA under basic medium. The synthesized materials showed worm-like pores and were more hydrothermally stable than MCM-41.[10] During that same time, Inagaki and co-workers also synthesized ethylene bridged PMO using 1,2-bis(trimethoxysilyl)ethane as silica source and octadecyltrimethylammonium chloride (C_{18}TMACl) as SDA.[11] The material showed high surface area (750 m^2/g) and pore diameter (3 nm) with 2D-hexagonal morphology.[11] So far, methylene, ethylene, phenylene, naphthylene, and thiophenylene organic groups have been successfully incorporated into the framework of PMO.[12,13] In 2002, Inagaki and his co-workers synthesized the first hybrid bi-functional PMO with crystal-like pore walls using 1,4-benzene

and 4,4'-biphenylene functional groups using alkyltrimethylammonium as SDA.[14] Additionally, Ozin and his co-workers synthesized highly branched periodic mesoporous dendrisilicas that has channel walls composed of interconnected dendrimer building blocks.[15] By varying organic bridging group, these materials can be used in various applications such as catalysis, sorption, bio-sensors, chromatography, and as molecular switches.[16,17,18,19,20]

Here, we have synthesized ethylene (EPMO) and phenylene (BPMO) bridged periodic mesoporous organosilicas via surfactant templating in an acidic medium. Additionally, co-condensation with organosilanes was used to synthesize functionalized BPMO and EPMO.

Experimental Section

Reagents: 4-(triethoxysilyl)butyronitrile (BN), Brij 76, and 1-pyrenecarboxylic acid (PCA) were purchased from Sigma Aldrich. 3-(aminopropyl)trimethoxysilane (AP), N-(2-aminoethyl)-3-aminopropyl-trimethoxysilane (AEAP), and Hydrochloric acid (HCl, 12.1 M) were purchased from Fisher. 3-(triethoxysilyl)propyl succinic anhydride (PSA), 1,4-bis(triethoxysilyl)benzene (BTEB), and bis(triethoxysilyl)ethane (BTEE) were purchased from Gelest. Ethyl alcohol (200 proof) was used for surfactant extraction in all syntheses. All the reagents were used as received without further purification.

Synthesis of BPMO. The material was synthesized using previously published method.[21] Brij 76 (0.5 g) was dissolved in 2 M HCl (12.5 mL, 25.0 mmol) and deionized water (2.5 mL) in a round bottom flask with continuous magnetic stirring for 30 min at 50 °C. BTEB (1.04 mL, 2.63 mmol) was then added to the mixture and the stirring was continued for another 20 h at 50 °C. The solid product was collected via filtration and was air-dried for 24 h. The surfactant template was removed by refluxing 1.0 g of dry solid with 150 ml of ethanol and conc. HCl (1.69 mL,

20.3 mmol) at 50 °C for 5 h. The surfactant removal step was repeated. The final product was filtered and air-dried for 24 h.

Synthesis of EMO. This material was prepared in the same way as BPMO but using BTEE (0.970 mL, 2.62 mmol) instead of BTEB as precursor. Because of a lower stability of this material it was hydrothermally treated at 100 ^{o}C for 48 h before performing solvent extraction.

Synthesis of Functionalized BPMO. These materials were prepared in the same way as BPMO, but adding dropwise an organosilane (AP (62.5 uL, 0.354 mmol), AEAP (77.2 uL, 0.354 mmol), ESA (99.8 uL, 0.354 mmol), or BN (84.8 uL, 0.354 mmol)) immediately after addition of BTEB (1.04 mL, 2.63 mmol). The molar ratio of BTEB : organosilane was 7.4:1. The final products were abbreviated as AP-BPMO, AEAP-BPMO, ESA-BPMO, and BN-BPMO.

Synthesis of Functionalized EPMO. These materials were prepared in the same way as EPMO, but adding dropwise an organosilane (AP (62.5 uL, 0.354 mmol), AEAP (77.2 uL, 0.354 mmol), ESA (99.8 uL, 0.354 mmol), or BN (84.8 uL, 0.354 mmol)) immediately after addition of BTEE (0.970 mL, 2.62 mmol). The molar ratio of BTEE : organosilane was 7.4:1. The white solid products were hydrothermally treated at 100^{o}C for 48 h before removing the surfactant. The final products were abbreviated as AP-EPMO, AEAP-EPMO, ESA-EPMO, and BN-EPMO.

Loading of 1-pyrenecarboxylic acid (PCA) on AP-BPMO or AEAP-BPMO. The materials were synthesized using previously published method.[22] A 3-fold excess of PCA (0.523 g, 2.12 mmol) (with respect to the nominal amine loading, 0.354 mmol g^{-1}) was added to 500 mg of AP-BPMO or AEAP-BPMO in anhydrous toluene (500 mL). The reaction mixture was refluxed in anhydrous toluene for 24 h under nitrogen atmosphere. The solid was then washed with 75 mL of toluene and THF to remove any physisorbed PCA. The material was then dried at 60 °C under high vacuum for 24 h for removal of solvent.

Characterization

Textural properties of support: Nitrogen sorption isotherms were obtained in a Micrometrics Tristar analyzer at -196^{o}C. Brunauer-Emmett-Teller (BET) and Barret-Joyner Halenda (BJH) methods were used to calculate surface area and pore size distribution, respectively. The samples were degassed under N_2 flow for 6 h at 100^{o}C prior to the analysis.

Powder X-ray diffraction: Small and wide-angle X-ray diffraction patterns were collected on a Bruker AXS D8 Discover powder diffractometer equipped with Cu Kα radiation (40 kV, 44 mA) over the range of 1–10° (low angle).

Diffuse reflectance infrared Fourier transform spectroscopy (DRIFT): A Bruker vertex 80 FTIR spectrophotometer was used to collect DRIFT spectra equipped with a HeNe laser and photovoltaic MCT detector and OPUS software. The samples were vacuum dried at 100^{o}C under Schlenk line for 24 h prior to analysis.

CHN elemental analysis: CHN elemental analysis was performed using Perkin Elmer 2100 Series II analyzer using acetanilide (ACE) as a calibration standard. The carbon materials were vacuum dried at 100^{o}C under Schlenk line for 12 h prior to analysis. Triplicate runs for each sample were performed.

Fluorescence Spectroscopy: The relative spacing of amine in amine functionalized BPMO and EMPO materials was studied using Cary Eclipse Fluorescence Spectrophotometer. PCA loaded samples (5 mg) were suspended in hexane (2.0 mL). The mixture was sonicated for 30 minutes. The suspensions were then excited at wavelength of 336 nm, emission was recorded in the range 350-600 nm. Fluorescence emission was scanned with both excitation and emission slit widths set at 5 nm.

Results & Discussions

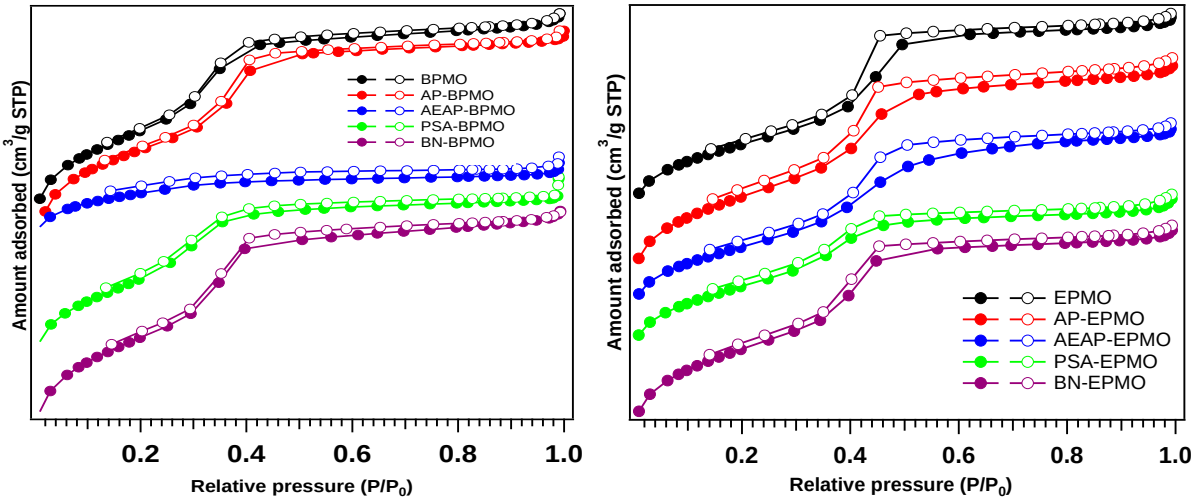

Figure 2: N_2 sorption isotherms of parent and functionalized BPMO (left) and EPMO (right)

Table 1: Structural properties and CHN elemental analysis of parent and functionalized BPMO and EPMO.

Material	Surface Area (m^2/g)	PSD (nm)	PV (cm^3/g)	N (mmol/g)
BPMO	941	3.6	0.70	-
AP-BPMO	921	3.0	0.65	0.65±0.15
AEAP-BPMO	572	2.9	0.30	0.79±0.10
PSA-BPMO	952	2.9	0.68	-
BN-BPMO	1126	2.9	0.82	0.47±0.05
EPMO	786	3.6	0.95	-
AP-EPMO	959	3.4	0.73	0.54±0.08
AEAP-EPMO	754	3.3	0.72	0.68±0.13
PSA-EPMO	729	3.1	0.58	-
BN-EPMO	972	3.3	0.80	0.38±0.06

The N_2 sorption isotherms of BPMO and EPMO with and without functional groups were type IV indicating mesoporous character of all the materials. The sharp increase in the adsorbed gas amount at P/P_0= 0.26-0.45 for all materials is due to the capillary condensation in the mesopores. The surface area, pore diameter and pore volume of the materials depend strongly on the type of organic bridging group and functionalities incorporated within the PMO structure. Most of the BPMOs had higher surface areas than the EPMOs suggesting the phenethyl bridging group was

more beneficial for the assembly of the mesostructures (Table 1). This may be due to the rigidity of the bridging group and to its capacity to interact with the protonated groups in the template via cation-π pairing. Small variations in surface areas and pore volumes were observed for most of the functionalized materials compared to the parent materials. These differences may be attributed to the effect of the functionalities on condensation rates and on the interaction with the template. The only large drop in these textural properties was observed for AEAP-BPMO (-40% in surface area and -58% in pore volume), which could be due to the effect of two amine groups per silane on the pH of the synthesis. Since the reaction is performed in acidic media, the high concentration of amines (twice as much as in AP-BPMO) it is more likely to have an effect on the pH dependent assembly of the supramolecular system. The drop was larger for BPMO suggesting interaction between the protonated amine and the phenylene ring may have competed with the interaction of the latter with the template. In contrast to the AEAP group, the BN group led to a significant enhancement in the textural properties of both PMOs. This remarkable effect may be due to the large dipole moment of the nitrile group, which likely favored the interaction with the template. While surface areas and pore volumes had smaller changes for most functionalized PMOs, the pore widths of all materials were clearly smaller than the parent PMOs. This decrease can be attributed to the space that the functional groups occupy inside of the pores.

Low angle XRD patterns of parent and functionalized PMOs were obtained over the range of 1–5° 2θ degrees (Figure 3). For parent EPMO, a sharp diffraction peak is observed at 1.7 2θ degrees followed by two small peaks at 2.3, and 2.5 2θ degrees. A strong diffraction peak is observed in range of 1.6-1.8 2θ degrees for BPMO with and without functional groups. Weak diffraction peaks at 3.2 and 3.4 2θ degrees are also observed for parent BPMO and BN-BPMO.

The diffraction patterns obtained suggest that all materials possess well-ordered 2D-hexagonal mesoporous structures. [23,24] Incorporation of functional group in the parent materials led to some degree of peak broadening, which is usually observed upon partial loss of structural ordering. The position of the (100) peak is shifted to higher 2θ ° in the functionalized materials, which is consistent with the decrease in pore width observed upon functionalization.

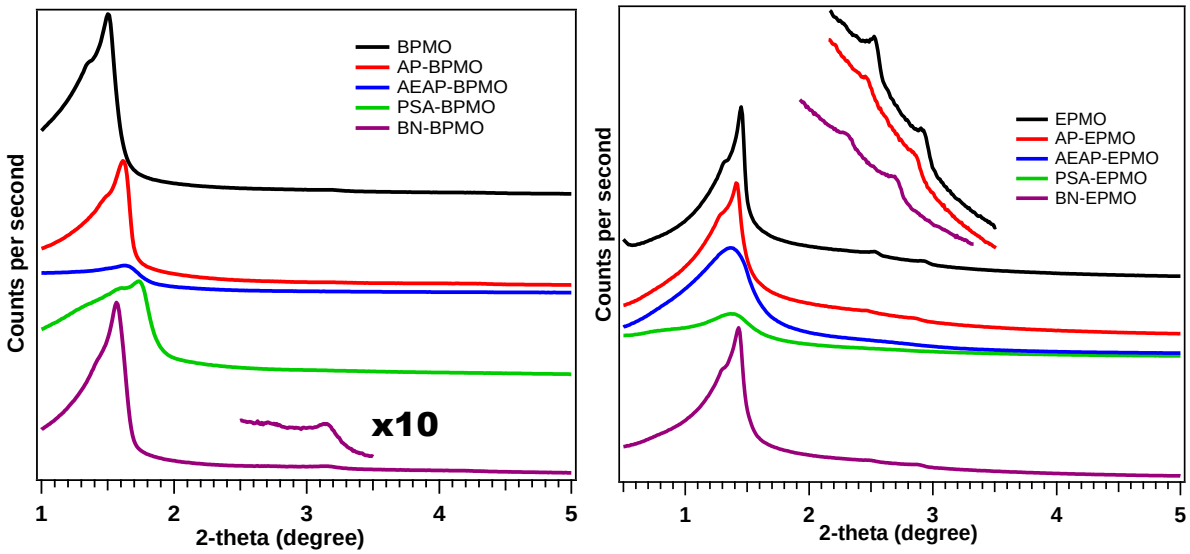

Figure 3: Low angle XRD patterns of parent and functionalized BPMO (left) and EPMO (right)

CHN elemental analysis (table 1) was performed on AP, AEAP, and BN functionalized BPMO and EPMO materials to quantify the amount of nitrogen, which is indicative of the amount of functional group present in each material. In general, slightly higher loads of groups were observed for BPMO than EPMO, which is consistent with a more efficient condensation process and more stable mesophases achieved with phenylene bridging groups. Because AEAP has two N per molecule, their actual loading is half of the N content. The data shows significantly lower amounts of AEAP loaded than of the other two groups, this is consistent with the more disruptive effect of AEAP on the synthesis of the materials.

DRIFT spectra of all PMO materials exhibited a strong broad band at 1030 cm^{-1} that is credited to the Si-O-Si stretching vibration of the materials' framework (Figure 4). Additionally, a broad band at 1200 cm^{-1} can be ascribed to Si-C stretching vibration in the ethane and phenylene

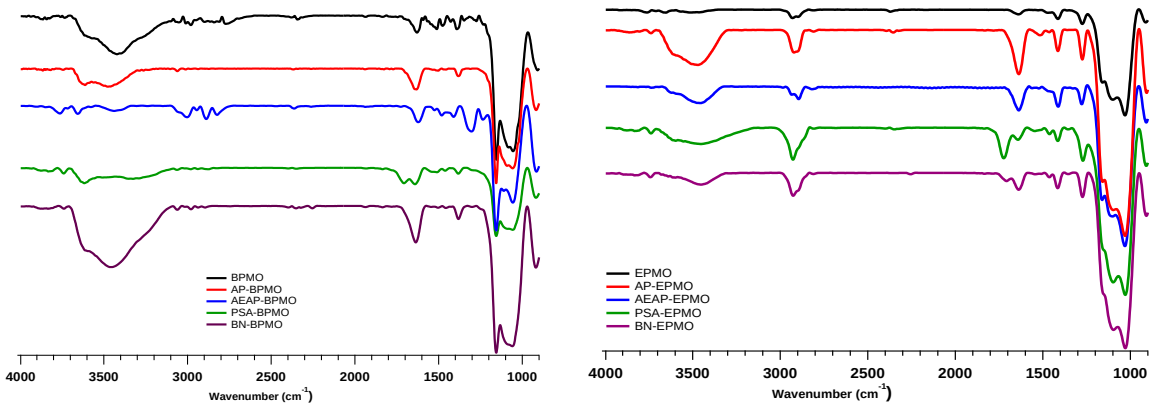

Figure 4: DRIFT spectra of parent and functionalized BPMO (left) and EPMO (right).

bridges and the organosilane functional groups.[25] All BPMO materials exhibit strong bands around 3100 and 1620 cm^{-1} corresponding to aromatic C-H and C=C bonds of the phenylene bridging group respectively.[26] A weak band around 2900 cm^{-1} is due to hydrocarbon chains from functional groups. All surfactant extracted materials exhibit a broad stretch between 3200-3400 cm^{-1} which is attributed to N-H or O-H stretching vibrations. All amine functionalized PMOs show a weak scissoring N-H band at 1620 cm^{-1}.[26] All succinic anhydride containing materials show a carbonyl stretching vibration at 1720 cm^{-1} assigned to carboxylic acids that result of hydrolysis of anhydride due to synthesis conditions.[27,28] A weak band is observed at 2240 cm^{-1} due to C≡N bond in butyronitrile functionalized materials.[29] Additionally a broad stretch between 3100-3700 cm^{-1} and a sharp band around 1700 cm^{-1} suggested some formation of -COOH due to the hydrolysis of C≡N.[27]

The distance between catalytically active functional groups such as amines is expected to play a crucial role in their performance. There have been different approaches reported to determine the

average distances between surface-immobilized amine groups including titration, solid-state NMR, and Biuret test.[30,31,32] All three techniques are used most commonly while dealing with

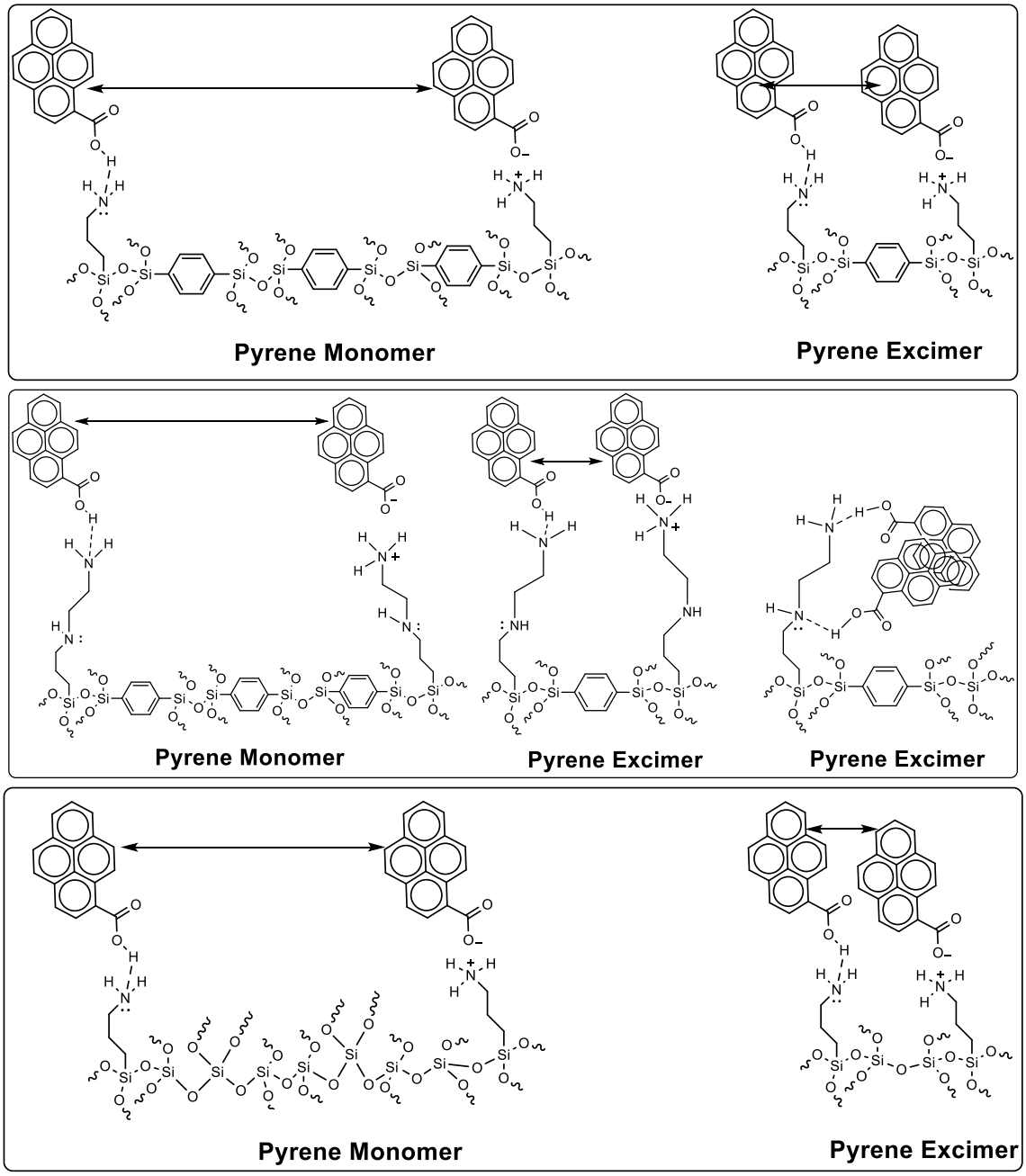

Figure 5: Possible interactions of PCA on different amine functionalized silica supports illustrating monomer and excimer emission

amino-acid incorporated materials. An alternative method to determine spatial isolation of amines is by coupling them with fluorophores and evaluating energy transfer processes between

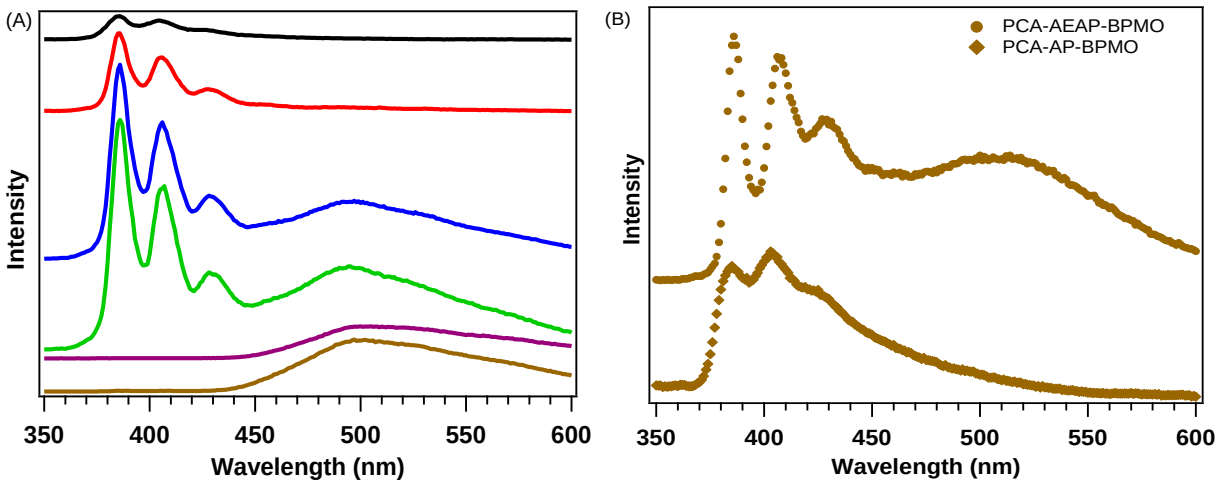

Figure 6: Fluorescence spectra of (A) PCA in solution at low (1.63 nM, top) to high (10.2 mM, bottom) concentration, emissions at ca. 380, 400 and 430 nm correspond to the monomer, and the broad emission at 500 nm indicate excimer formation; and (B) PCA-AP-BPMO (◆), and PCA-AEAP-BPMO (●) in hexane. The mixtures were excited at λ = 336 nm.

the attached fluorophores.[32] When the fluorophore is a polyaromatic molecule like pyrene, the individual molecules give a different fluorescence signature than when they are π-stacked forming an excimer.[33,34] Winnik reported the formation of pyrene excimer upon excitation if two pyrene molecules are located within 0.3-1 nm distance.[33] Thus, by pairing PCA with amine groups in AP-BPMO and AEAP-BPMO, we can establish whether the groups are close (< 1 nm) or far away (>1 nm) from each other depending on whether we observe the excimer peak or not. Figure 5 shows the possible interactions that could take place between PCA and amine functional groups. The carboxylic acid can interact with amine groups via hydrogen bonding or ionic bonding.[35] Fluorescence spectra of PCA suspensions in hexane excited at 336 nm (Figure 6A) show the emission wavelengths of monomer at low concentrations and excimer at high concentrations. All PCA probed materials at equimolar concentrations showed three distinct peaks related to pyrene monomers at λ = 384, 408, and 430 nm. Additionally, only AEAP showed a new broad peak at λ = 520 nm at equimolar concentrations of all the materials, suggesting excimer formation from stacking of PCA molecules. As shown in Figure 5, PCA can

interact either with two different di-amine groups or with two nitrogen atoms located on the functional groups, and this may be the reason for the small excimer peak observed. We expect the relative distance between organic functionalities to be helpful information to synthesize metal-ligand complexes for catalysis.

Conclusions

In summary, we successfully synthesized ethylene and phenylene bridged PMOs and introduced different organic functionalities within the silica framework via co-condensation between organo-bis-silanes and functional organo-mono-silanes under acidic conditions. Parent and functionalized EPMO and BPMO materials showed type IV isotherm behavior confirming mesoporosity, and their XRD diffraction patterns suggested their mesopores were ordered in 2D hexagonal arrays. However small variations in the structural properties of the materials can be observed upon incorporation of organic functional groups within the framework. These differences were attributed to interferences of some of the functionalities with the mesophase formation due to changes in pH or competing interactions with the template. The presence of different organic functionalities was verified using DRIFT spectroscopy and elemental (CHN) analysis. The spectra showed the characteristic bands for N-H (3200-3400 cm^{-1}, 1620 cm^{-1}), C=O (1720 cm^{-1}), and C≡N (2240 cm^{-1}), and elemental analysis indicated N-containing organic groups were incorporated at loadings between 0.3 and 0.7 mmol g^{-1}. Probing the spatial distribution of amines with PCA indicated monomer formation for AP-BPMO suggesting amine groups are isolated in this material. In contrast, excimer formation in AEAP-BPMO suggested that either the groups may be close enough to interact with each other, or that PCA interacted with the two amine groups of the same AEAP functionality.

References

[1] Kresge, C.; Lenowicz, M.; Roth, W.; Vartuli, J.; Beck, J. Ordered Mesoporous Molecular Sieves Synthesized by a Liquid-Crystal Template Mechanism, *Nature*, **1992**, *359*, 710-712.

[2] Moller, K.; Bein, T. Inclusion Chemistry in Periodic Mesoporous Hosts, *Chem. Mater.*, **1998**, *10*, 2950-2963.

[3] Bharti, C.; Nagaich, U.; Pal, A.; Gulati, N. Mesoporous Silica Nanoparticles in Target Drug Delivery System: A Review, *Int. J. Pharma. Investig.*, **2015**, *5*, 124-133.

[4] Dana, E. Adsorption of Heavy Metals on Functionalized-Mesoporous Silica: A Review, *Micro. and Meso. Mat.*, **2017**, *247*, 145-157.

[5] Shylesh, S.; Prinson, P.; Sisodiya, S.; Singh, A. Periodic Mesoporous Silica and Organosilicas: An Overview Towards Catalysis, *Catal. Surv. Asia*, **2008**, *12*, 266-282.

[6] Liang, Z.; Mohanty, P; Fei, Y.; Landskron, K. Synthesis of Corsite Nanocrystals from Ethane Bridged Periodic Mesoporous Organosilica at Low Temperature and Extreme Pressure, *Chem. comm.*, **2010**, *46*, 8815-8817.

[7] Wang, W.; Lofgreen. J.; Ozin, G. Why PMO? Towards Functionality and Utility of Periodic Mesoporous Organosilicas, *Small*, **2010**, *6, 23*, 2634-2642.

[8] Hatton, B.; Landskron, K.; Whitnall, W.; Perovic, D.; Ozin, G. A. Past, Present and Future of Periodic Mesoporous Organosilica – The PMOs, *Acc. Chem. Res.*, **2005,** *38*, 305-312.

[9] Asefa, T.; Maclachlan, M.; Coombs, N.; Ozin, G. Periodic Mesoporous Organosilicas with Organic Groups Inside the Channel Walls, *Nature*, **1999**, *402*, 867-871.

[10] Melde, B.; Holland, B.; Blanford, C.; Stein, A. Mesoporous Sieves with Unified Hybride Inorganic/Organic Frameworks, *Chem. Mater.*, **1999**, *11*, 3302-3308.

[11] Inagaki, S.; Guan, S.; Fukushima, Y.; Ohsuna, T.; Terasaki, O. Novel Mesoporous Materials with a Uniform Distribution of Organic Groups and Inorganic Oxide in Their Frameworks, *J. Am. Chem. Soc.*, **1999**, *121*, 9611-9614.

[12] Hoffmann, F.; Cornelius, M.; Morell, J.; Fröba, M. Silica-Based Mesoporous Organic–Inorganic Hybrid Materials, *Angew. Chem. Int. Ed.*, **2006**, *45*, 3216-3251.

[13] Hatton, B.; Landskron, K.; Whitnall, W.; Perovic,D.; Ozin, G. Spin-Coated Periodic Mesoporous Organosilica Thin Films—Towards a New Generation of Low-Dielectric-Constant Materials, *Adv. Funct. Mater.*, **2005**, *15*, 823-829.

[14] Inagaki, S.; Guan, S.; Ohsuna, T.; Terasaki, O. An Ordered Mesoporous Organosilica Hybrid Material with a Crystal-Like Wall Structure, *Nature*, **2002**, *416*, 304-307.

[15] Landskron, K.; Ozin, G. Periodic Mesoporous Dendrisilica, *Science*, **2004**, *306*, 1529-1532.

[16] Yuan, X.; Lee, H.; Kim, J.; Yie, J.; Kim, J. Periodic Mesoporous Organosilicas Functionalized with Sulfonic Acid Group. Synthesis and Alkylation of Phenol, *Chem. Lett.*, **2003**, *32*, *7*, 650-651.

[17] Yang, Q.; Kapoor, M.; Inagaki, S.; Shirokura, N.; Kondo, J.; Domen, K. Catalytic Application of Sulfonic Acid Functionalized Mesoporous Benzene-Silica with Crystal-Like Pore Wall Structure in Esterification, *J. Mol. Catal.*, **2005**, *230*, 85-89.

[18] Gao, M.; Han, S.; Hu, Y.; Dynes, J.; Liu, X.; Wang, D. A pH-Driven Molecular Shuttle Based on Rotaxane-Bridged Periodic Mesoporous Organosilicas with Responsive Release of Guests, *RSC Adv.*, **2016**, *6*, 27922-27932.

[19] Wu, C.; Liang, Y.; Yang, K.; Min, Y.; Liang, Z.; Zhang, L.; Zhang, Y. Clickable Periodic Mesoporous Organosilica Monolith for Highly Capillary Chromatographic Separation, *Anal. Chem.*, **2016**, *88*, 1521-1525.

[20] Waki, M.; Maegawa, Y.; Hara, K.; Goto, Y.; Shirai, S.; Yamada, M.; Mizoshita, N.; Tani, Takao.; Chun, W.; Muratsugu, S.; Tada, M.; Fukuoka, A.; Inagaki, S. A Solid Chelating Ligand: Periodic Mesoporous Organosilica Containing 2, 2'-Biprydine within the Pore Walls, *J. Am. Chem. Soc.*, **2014**, *136*, 4003-4011.

[21] Wang, W.; Zhou, W.; Sayari, A. Synthesis of Periodic Mesoporous Phenylenesilica under Acidic Conditions with Novel Molecular Order in the Pore Walls, *Chem. Mater.*, **2003**, *15*, 4886-4889.

[22] Hicks, J.; Dabestani, R.; Buchanan III, A.; Jones, C.; Spacing and Site Isolation of Amine Groups in 3-Aminopropyl-Grafted Silica Materials: The Role of Protecting Groups, *Chem. Mater.*, **2006**, *18*, 5022-5032.

[23] Sadasivan, S.; Khushalani, D.; Mann, S. Synthesis and Shape Modification of Organo-Functionalized Silica Nanoparticles with Ordered Mesostructured Interiors, *J. Mater. Chem.*, **2003**, *13*, 1023-1029.

[24] Burleigh, M.; Markowitz, M.; Spector, M.; Gaber, B. Direct Synthesis of Periodic Mesoporous Organosilicas: Functional Incorporation by Co-condensation with Organosilanes, *J. Phys. Chem. B*, **2001**, *105*, 9935-9942.

[25] Wahab, M.; Kim, I.; Ha, C. Hybrid Periodic Mesoporous Organosilica Materials Prepared from 1,2-Bis(triethoxysilyl)ethane and (3-Cyanopropyl)triethoxysilane, *Micro. & Meso. Mat.*, **2004**, *69*, 19-27.

[26] Abboud, M.; Sayari, A. Novel Family of Periodic Mesoporous Organosilicas Containing Azobenzene within the Pore Walls, *Micro. & Meso. Mat.*, **2017**, *249*, 157-164.

[27] Fiorilli, S.; Camarota, B.; Perrachon, D.; Bruzzoniti, M.; Garrone, E.; Onida, B. Direct Synthesis of Large-Pore Ethane-Bridged Mesoporous Organosilica Functionalized with Carboxylic Groups, *Chem. Commun.*, **2009**, 4402-4404.

[28] Barabanova, A.; Pryakhina, T.; Afanas'ev, E.; Zavin, B.; Vygodskii, Y.; Askadskii, A.; Philippova, O.; Kholkhlov, A. Anhydride Modified Silica Nanoparticles: Preparation and Characterization, *Appl. Surf. Sci.*, **2012**, *258*, *7*, 3168-3172.

[29] Fiorilli, S.; Onida, B.; Barbara, B.; Edoardo, G. In Situ Infrared Study of SBA-15 Functionalized with Carboxylic Groups Incorporated by a Co-Condensation Route, *J. Phys. Chem. B*, **2005**, *109*, 16725-16729.

[30] Drochioiu, G.; Damoc, N.; Przybylski, M. Novel UV Assay for Protein Determination and Characterization of Copper-Protein Complexes by Mass Spectrometry, *Talanta*., **2006**, *69*, 556-564.

[31] May, F.; Church, S.; Major, S.; Westley, B. The Closely Related Estrogen-Regulated Trefoil Proteins TFF1 and TFF3 have Markedly Different Hydrodynamic Properties, Overall Charge and Distribtuion of Surface Charge, *Biochem.*, **2003**, *42*, 8250-8259.

[32] Hashidzume, A.; Harada, A. Steady-State Fluorescence and NMR Study of Self-Association Behavior of Poly(methacrylamide) Bearing Hydrophobic Amino-Acid Residues, *polymer*, **2005**, *46*, 1609-1616.

[33] Winnik, F. Photophysics of Preassociated Pyrenes in Aqueous Polymer Solutions and in Other Organized Media, *Chem. Rev.*, **1993**, *93*, 587-614.

[34] Bass, J.; Katz, A. Thermolytic Synthesis of Imprinted Amines in Bulk Silica, *Chem. Mater.* **2003**, *15*, 2757-2763.

[35] Hicks, J.; Jones, C. Controlling the Density of Amine Sites on Silica Surfaces Using Benzyl Spacers, *Langmuir*, **2006**, *22*, 2676-2681.

CHAPTER 4

GENERAL CONCLUSIONS

The primary focus of this work was the synthesis of two different types of mesoporous materials: nitrogen-doped ordered mesoporous carbon (N-OMC) and functionalized periodic mesoporous organosilica (PMO), their characterization and their potential applications.

My research on N-OMC focused on its synthesis, characterization, and its use as an active catalyst for hydrogenation of nitrobenzene. I presented novel synthetic method to synthesize N-OMC based on the condensation of 3-aminophenol and formaldehyde using Pluronic F127 as the structure directing agent (SDA) in basic medium. The developed procedure is much simpler, low-cost, convenient, and suitable for large-scale industrial productions compare to that of post-synthetic and nanocasting route. Additionally, the synthesis procedure allows direct incorporation and homogeneous distribution of nitrogen functionalities within the carbon framework. Based on N_2 physisorption studies, we learned that the material exhibited high surface area, pore volumes and had narrow pore size distributions. The material was then used to support Pd nanoparticles via impregnation followed by reduction using $NaBH_4$/EtOH solution. FTIR and XPS results suggested the formation of pyrolic, and pyridinic N functionalities at higher carbonization temperatures that are also responsible for uniform dispersion of palladium nanoparticles compared to that of Pd-OMC due to stronger metal-support interactions. Pd-N-OMC materials showed better catalytic activity for hydrogenation of nitrobenzene compared to that of Pd-OMC materials. Based on these results, it is reasonable to conclude that the better catalytic activity for hydrogenation of nitrobenzene is due to nitrogen functionalities that are incorporated within the carbon framework. These findings open a new direction to investigate catalytic selectivity for hydrogenation of nitrobenzene.

In chapter 3, the synthesis of ethylene and phenylene bridged PMO functionalized with various organic groups was described. The materials were synthesized via co-condensation between organo-mono-silanes and organo-bis-silanes. The parent- and functionalized-EPMO, and BPMO materials exhibited high surface area, pore volume, and pore sizes. The materials presented diffraction peaks that correspond to 2D-hexagonal pore structure. Small differences in textural properties of the functionalized materials were attributed to interferences of some of the functionalities with the mesophase formation. Fluorescence spectroscopy using PCA as a probe was used to analyze the relative distance between amine groups in amine functionalized materials. The PCA-AP-BPMO showed only peaks corresponding to monomer formation, suggesting the AP groups are spatially isolated at least 1 nm apart from each other. In contrast, formation of the excimer peak in PCA-AEAP-BPMO could be attributed to interactions taking place between PCA molecules in two nitrogen functionalities of the same AEAP group or two different AEAP functional groups. We believe these functional materials have ideal properties for advanced applications such as interfacial catalysis and selective adsorption.